Vaccine plus microbicide effective in preventing vaginal SIV transmission in macaques

Mohammad Arif Rahman [1,10], Massimiliano Bissa [1,10],
Isabela Silva de Castro[1,10], Sabrina Helmold Hait[2,10], James D. Stamos[1],
Farzana Bhuyan[3], Ruth Hunegnaw[2], Sarkis Sarkis[1], Anna Gutowska [1],
Melvin N. Doster[1], Ramona Moles[1], Tanya Hoang[2], Lisa M. Miller Jenkins [4],
Ettore Appella [5], David J. Venzon [6], Hyoyoung Choo-Wosoba[6],
Timothy Cardozo [7], Marc M. Baum [8], Daniel H. Appella[9],
Marjorie Robert-Guroff[2] & Genoveffa Franchini [1] ✉

The human immunodeficiency virus epidemic continues in sub-Saharan Africa, and particularly affects adolescent girls and women who have limited access to antiretroviral therapy. Here we report that the risk of vaginal simian immunodeficiency virus (SIV)$_{mac251}$ acquisition is reduced by more than 90% using a combination of a vaccine comprising V1-deleted (V2 enhanced) SIV envelope immunogens with topical treatment of the zinc-finger inhibitor SAMT-247. Following 14 weekly intravaginal exposures to the highly pathogenic SIV$_{mac251}$, 80% of a cohort of 20 macaques vaccinated and treated with SAMT-247 remained uninfected. In an arm of 18 vaccinated-only animals without microbicide, 40% of macaques remained uninfected. The combined SAMT-247/vaccine regimen was significantly more effective than vaccination alone. By analysing immune correlates of protection, we show that, by increasing zinc availability, SAMT-247 increases natural killer cytotoxicity and monocyte efferocytosis, and decreases T-cell activation to augment vaccine-induced protection.

Although available treatments have reduced new HIV infections from the peak level of 3.2 million recorded in 1996 by 54% in 2021, infection with human immunodeficiency virus (HIV) continues to cause substantial morbidity and mortality. An estimated 1.5 million people worldwide acquired HIV in 2021 (ref. 1). Women are not only biologically more susceptible to HIV-1 infection than men, but they are often socially and culturally more vulnerable to infection as well[1]. Approximately 5,000 women aged 15–24 years are infected with HIV every week globally, and in sub-Saharan Africa six out of seven new HIV infections in adolescents occur in girls[1,2]. An effective HIV vaccine is urgently needed,

[1]Animal Models and Retroviral Vaccines Section, National Cancer Institute, Bethesda, MD, USA. [2]Section on Immune Biology of Retroviral Infection, National Cancer Institute, Bethesda, MD, USA. [3]Translational Autoinflammatory Diseases Section, Laboratory of Clinical Immunology and Microbiology, National Institute of Allergy and Infectious Diseases, National Institutes of Health, Bethesda, MD, USA. [4]Collaborative Protein Technology Resource, Laboratory of Cell Biology, National Cancer Institute, Bethesda, MD, USA. [5]Chemical Immunology Section, National Cancer Institute, Bethesda, MD, USA. [6]Biostatistics and Data Management Section, Center for Cancer Research, National Cancer Institute, Bethesda, MD, USA. [7]New York University School of Medicine, NYU Langone Health, New York, NY, USA. [8]Oak Crest Institute of Science, Monrovia, CA, USA. [9]Synthetic Bioactive Molecules Section, National Institute of Diabetes and Digestive and Kidney Diseases, National Institutes of Health, Bethesda, MD, USA. [10]These authors contributed equally: Rahman, M. A., Bissa, M., Silva de Castro, I., Helmold Hait, S. ✉e-mail: franchig@mail.nih.gov

and specifically one to reduce the burden of disease in women and curb the HIV epidemic.

Of the nine clinical HIV vaccine efficacy trials carried out in humans so far[3–12], only the RV144 canarypox-based (ALVAC) vaccine demonstrated a modest degree of equivalent efficacy in males and females[8]. The ALVAC-based/gp120/alum vaccine platform, which encodes virus-like particles, reduced virus acquisition by 31.2% in humans in a phase III efficacy trial[8].

The macaque model has convincingly demonstrated the pre-clinical potential of the ALVAC/simian immunodeficiency virus (SIV) vaccine modality boosted with gp120 (ref. 13) by reproducing the efficacy of the successful RV144 HIV vaccine trial testing the alum adjuvant[8] and predicting the failure of the HVTN-702 trial in South Africa, using the MF59 adjuvant[10]. Moreover, work in this model has demonstrated that the efficacy of ALVAC-based HIV vaccine candidates can be improved by using a DNA prime[14], simplifying the vaccine regimen[15], and by better exposing the α-helical conformation of variable region 2 (V2) via the deletion of V1 (ref. 16). In vaccinated macaques, V2-specific ADCC correlated with decreased risk of virus acquisition[16] consistent with the primary and secondary correlates of risk in RV144 (ref. 17). Both human and macaque antibodies recognizing the α-helical conformation of V2 inhibit V2-mediated CD4^{+} T-cell co-stimulation and CCR5 expression[18]. Systems biology and functional analyses of CD14^{+} cells in vaccinated macaques demonstrated that the efficacy of the improved DNA/ALVAC gp120/alum platform results from the engagement of the CCR2/CCL2 anti-inflammatory axis[15,19], activation of the c-AMP/CREB1 pathway in anti-inflammatory (M2-like) monocytes[20] and monocyte efferocytosis[15,21] necessary for the clearance of apoptotic cells[22]. In addition, in macaques the vaccine-induced recruitment of NKp44 IL-17^{+} cells to mucosal sites and the decreased expression of CCR5 on Th1 and Th2 cells are also correlates of decreased risk of virus acquisition[13,14,23].

Thus, while the main immune correlates of risk are increasingly understood, the efficacy of the ΔV1DNA/ALVAC/ΔV1gp120/alum vaccine regimen remains suboptimal in both female and male macaques, decreasing the per/exposure risk of virus acquisition by an average of 70%, and protecting approximately half of vaccinated animals from SIV_{mac251} acquisition[15]. The SAMT-247 (S-acyl-2-mercaptobenzamide thioester) microbicide notably targets the mutationally intolerant HIV nucleocapsid (NC) protein zinc fingers[24] and, by acetylating the cysteine sidechains of the NC protein, causes zinc ejection and loss of virus infectivity[25,26]. Importantly, SAMT-247 exhibits an intracellular recycling mechanism whereby released thiol is re-acetylated by acetyl-CoA, resulting in generation of a reactive thioester compound, thus allowing for numerous rounds of virucidal activity[27].

The SAMT class of compounds has prevented HIV transmission in vitro in cell-based assays, in explant cultures and to varying degrees in transgenic mice and macaques[28–31]. In this Article, we evaluated whether the SAMT microbicide could increase the potency of an RV144-like vaccine in macaques and its potential suitability for use in human trials, as no other vaccine platforms has yet been clinically effective in humans[3–12].

We observed a substantial synergy between the microbicide and the engineered V1-deleted envelope immunogens, delivered by the DNA/ALVAC vaccine platform[15,16]; the combined approach reduced the risk of SIV infection in female macaques by more than 90%. SAMT-247, a zinc finger protein inhibitor with virucidal activity, unexpectedly also augmented vaccine-induced protective responses, probably by increasing zinc availability. We propose that our pre-clinical study charts a viable path towards effectively preventing HIV transmission in women.

Results

Mucosal microbicide reduces SIV_{mac251} acquisition
We designed a study in macaques powered to dissect the differences between vaccination alone or vaccination plus SAMT-247 treatment,

based on the reproducible efficacy of the ΔV1DNA/ALVAC-SIV/ΔV1gp120/alum vaccine in decreasing the risk of SIV_{mac251} acquisition by 60–70% (refs. 15,16). We administered the vaccine regimen to 38 female macaques. Five weeks after the last immunization (week 17), all animals were exposed to up to 14 weekly intravaginal SIV_{mac251} challenges. Four hours before each challenge exposure, 20 vaccinated animals were treated vaginally with 0.8% SAMT-247 in hydroxyethyl cellulose (HEC) gel, and the remaining 18 animals with HEC gel only. Two additional groups of non-immunized animals (six each) were treated either with SAMT-247/HEC gel or HEC gel at 4 h before viral exposure as controls (Fig. 1a). All animals were challenged until infection was documented by repeated nanodroplet PCRs. We designed the study to include SIV acquisition data from 31 historical controls (Online Methods) challenged with the same stock of virus in the same animal facility. Vaccine efficacy (VE) was measured as per-exposure risk of SIV acquisition. As expected, no difference in the risk of virus acquisition was observed between concurrent and historical controls (Extended Data Fig. 1a). Vaccine alone significantly (65%) decreased the risk of virus acquisition compared with all controls ($P = 0.0074$; Fig. 1b), as well as only historical controls ($P = 0.0061$; Extended Data Fig. 1b), consistent with prior studies[15]. In addition, a trend was observed using only the six concurrent controls (Extended Data Fig. 1c). Strikingly, the vaccine + SAMT-247 combination afforded a 92.7% reduction in the risk of virus acquisition when compared with all controls ($P < 0.0001$; Fig. 1c), as well as with concurrent or historical controls separately ($P = 0.0002$ and $P < 0.0001$, respectively; Extended Data Fig. 1d,e). The vaccine + SAMT-247 combination differed significantly from the vaccine-only group ($P = 0.006$; Fig. 1d) and protected 16 of 20 animals (80%) from infection. In contrast, treatment with SAMT-247 alone did not significantly decrease the risk of virus acquisition when compared with combined controls (Fig. 1e) or the concurrent or historical controls separately (Extended Data Fig. 1f,g). In vaccinated animals that became infected, we observed lower levels of virus RNA in plasma 2 weeks post-infection, regardless of SAMT-247 treatment, but this was not sustained (Fig. 1f).

SAMT-247 modulates in vitro NK cell functions
Immune correlates of reduced risk elicited by the DNA/ALVAC/gp120/alum vaccine platform include systemic V2-specific ADCC[16] mucosal envelope-specific NKp44^{+} cells producing IL-17 (ref. 13), CD14^{+} monocytes mediating efferocytosis[15] and Th1/Th2 cells expressing no or low levels of CCR5 (refs. 14–16). We tested the immune correlates of risk separately in vaccinated and vaccinated + SAMT-247-treated groups.

The levels of systemic antibodies to ΔV1gp120 and V2 peptides, ADCC titres and V2-specific ADCC, measured using a competitive assay with F(ab')2 obtained from anti-V2 mAbs NCI05 or NCI09, did not differ in the vaccinated SAMT-247-treated or untreated groups, as expected (Extended Data Fig. 2a–e). Surprisingly, specific ADCC activity and titres at the end of immunization (week 17) correlated significantly with decreased risk of SIV_{mac251} acquisition in the vaccine-only group ($R = 0.67$, $P = 0.002$ and $R = 0.60$, $P = 0.009$, respectively; Extended Data Fig. 2f,g), but not in the vaccine+SAMT-247 group (Extended Data Fig. 2h,i). The same was observed for V2-specific ADCC defined by NCI05 and NCI09 F(ab')2 ($R = 0.75$, $P = 0.0003$ and $R = 0.77$, $P = 0.0002$, respectively; Extended Data Fig. 2j–m). These findings raised the hypothesis that SAMT-247 treatment may have affected mucosal ADCC responses in vivo at the time of virus exposure.

As mucosal samples from vaccinated animals were not available, we tested this hypothesis by treating human PBMCs with SAMT-247 as effector cells in vitro before setting up the ADCC assays. We found that treatment with SAMT-247 in vitro significantly augmented ADCC activity mediated by plasma antibodies (week 17) from vaccinated animals ($P < 0.0001$; Fig. 2a). The difference in ADCC activity in vitro measured in the presence or absence of SAMT-247 correlated with decreased risk of virus acquisition in vivo in the vaccinated + SAMT-247-treated
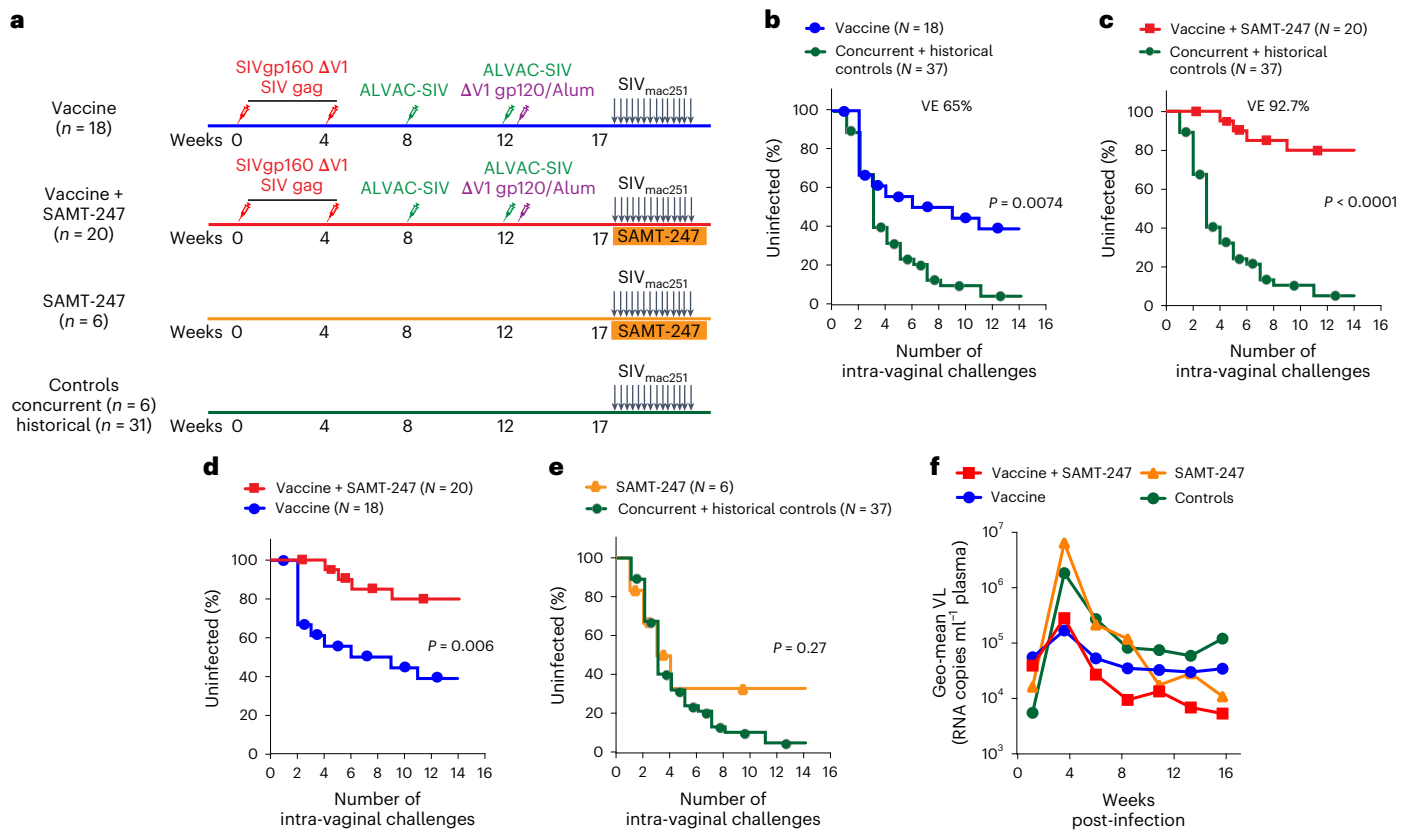
Fig. 1 | Immunization regimen, infection rate and SIV plasma virus. a, Rhesus macaques were subdivided into four groups: vaccine ($n = 18$), vaccine + SAMT-247 ($n = 20$), SAMT-247 ($n = 6$), and concurrent and historical controls ($n = 6$ and 31). Thirty-eight animals were primed with ΔV1 DNA-SIVgp160+p57 Gag and boosted with ALVAC-SIV encoding *env*, *gag* and *pol* and ALVAC-SIV + ΔV1 gp120 protein in alum hydroxide at the indicated timepoints. Twelve animals remained naïve until SIV challenge. Beginning at week 17, vaccine efficacy (VE) was assessed by subjecting all animals to up to 14 weekly intravaginal viral exposures (arrows) in the presence or absence of SAMT-247 until infection was confirmed. Animals either received 0.8% SAMT-247 in HEC gel ($n = 26$) or HEC gel only ($n = 24$) 4 h before each low-dose SIV$_{mac251}$ challenge. **b,c**, Significant protection in the vaccine group ($P = 0.0074$) (**b**) and the vaccine + SAMT-247 group ($P < 0.0001$) (**c**) compared with concurrent + historical controls. **d**, Delayed SIV acquisition in the vaccine + SAMT-247 group compared with the vaccine-only group ($P = 0.006$). **e**, No differences in delayed acquisition in the SAMT-247 group were observed compared with the combined concurrent plus historical controls ($P = 0.27$). **f**, Viral load (VL) geometric means of all macaque groups over time. Productive infection was qualified by the presence of viral DNA and RNA in mucosa and persistence of viral RNA in plasma over time. Data shown in **b**–**e** were analysed with log-rank (Mantel–Cox) test.

animals ($R = 0.50$, $P = 0.024$; Fig. 2b). Since these data suggest that topical administration of SAMT-247 may have augmented mucosal natural killer (NK) effector function, we tested whether SAMT-247 also affects mucosal NK function following in vitro PMA (phorbol 12-myristate 13-acetate)/Ionomycin stimulation. For simplicity, PMA/Ionomycin stimulation is referred to as PMA stimulation in this publication. We found that SAMT-247 increased granzyme B and perforin expression ($P = 0.02$ for both; Fig. 2c), and decreased IFN-γ ($P = 0.02$) and TNF-α (not significant (NS)) in macaque mucosal NKG2A⁺ cells (Fig. 2d). A similar effect was also observed in human NK cells from blood (Extended Data Fig. 3a,b). Next, we measured mucosal envelope-specific NKp44⁺IL-17⁺ cells, another correlate of decreased risk of virus acquisition[13,23], and found that their frequency did not differ in the vaccinated/ SAMT-247-treated or untreated groups at week 13, as expected, since at this timepoint no SAMT-247 had been administered (Extended Data Fig. 3c). Interestingly, however, their frequency correlated significantly with decreased risk of virus acquisition in the vaccinated-only group ($R = 0.77$, $P = 0.0002$; Extended Data Fig. 3d), suggesting that this response in the mucosa may have been modulated by SAMT-247 treatment. We tested this hypothesis on mucosal mononuclear cells isolated from nine age-matched macaques by pre-treating them in vitro with PMA with and without SAMT-247. The percentage of NKp44⁺ cells producing IL-17 following PMA stimulation was increased by SAMT-247

($P = 0.04$; Fig. 2e and Extended Data Fig. 3e,f), supporting the hypothesis that in vivo mucosal treatment with SAMT-247 locally augments the function of NKp44⁺ cells, thereby increasing mucosal integrity and enhancing vaccine efficacy. Collectively, these data suggest that SAMT-247 synergizes with vaccination by increasing NKG2A function and ADCC as well as mucosal protective NKp44⁺ producing IL-17.

CD14⁺ cell function is increased by SAMT-247

CD14⁺ cell-associated efferocytosis is an innate CD14⁺ monocyte response essential for the clearance of apoptotic cells, maintenance of tissue homeostasis and eradication of pathogens[32]. Vaccine-induced CD14⁺ cell-mediated efferocytosis measured in blood correlated with a reduced risk of virus acquisition in the vaccinated-only group ($R = 0.62$; $P = 0.01$; Fig. 2f), as observed in prior studies with this vaccine regimen[15], but not in the vaccinated/SAMT-247-treated group (Extended Data Fig. 3g). This raised the hypothesis that SAMT-247 may also affect macrophage functionality at the mucosal site. We therefore performed an efferocytosis assay with the cryopreserved ex vivo CD14⁺ cells purified from blood of vaccinated animals (week 14) in the presence and absence of SAMT-247 and found that SAMT-247 did indeed augment both the percentage of CD14⁺ cells engulfing apoptotic cells as well as the per-cell amount of engulfed apoptotic cells measured as mean fluorescence intensity (MFI) within CD14⁺ cells collected before (pre-)
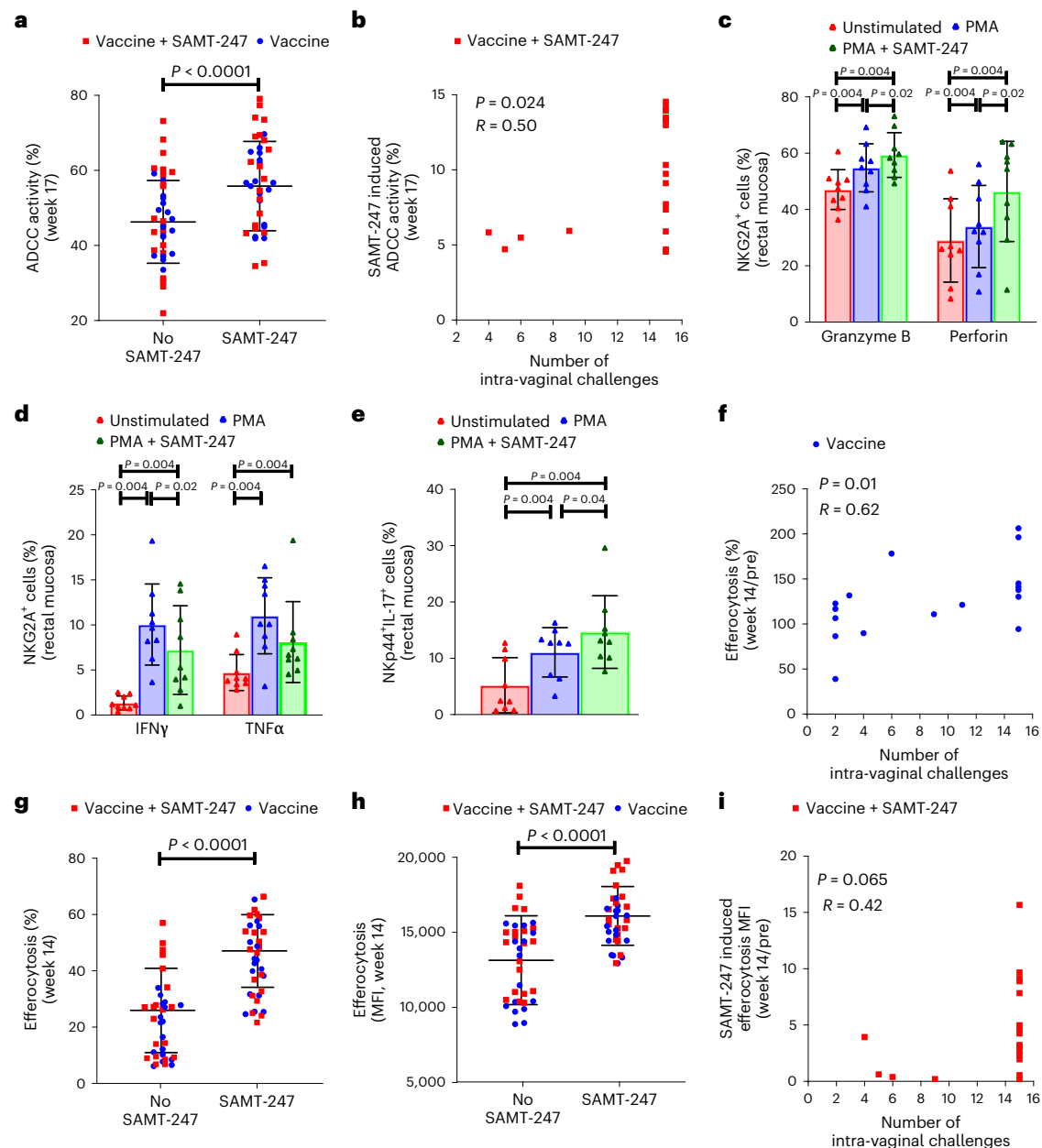
Fig. 2 | ADCC and NK responses and efferocytosis ex vivo and/or in vitro.
a, Comparison of SAMT-247 non-treated/treated effector cell-mediated ADCC activity in the vaccine ($n = 18$) and vaccine + SAMT-247 groups ($n = 20$; $P < 0.0001$). **b**, Correlation of SAMT-247-induced ADCC activity with number of intravaginal challenges in the vaccine + SAMT-247 group ($n = 20$; $P = 0.024$). **c,d**, Intracellular Granzyme B, perforin, IFN-γ and TNF-α in macaque rectal mucosal ($n = 9$) NKG2A+ cells in the presence or absence of different stimuli. **e**, Macaque rectal mucosal NKp44+IL-17+ cells in the presence or absence of different stimuli ($n = 9$). **f**, Correlation of efferocytosis with number of intravaginal challenges in animals in the vaccine group ($n = 18$; $P = 0.01$). **g,h**, Comparison of percentage of efferocytosis ($P < 0.0001$) (**g**) and efferocytosis MFI ($P < 0.0001$) (**h**) using week 14 CD14+ monocytes in all vaccinated animals ($n = 38$). **i**, Correlation of SAMT-247-induced efferocytosis (SAMT-247-untreated efferocytosis subtracted from SAMT-247-treated efferocytosis) with number of intravaginal challenges in the vaccine + SAMT-247 group ($n = 20$; $P = 0.065$). Data shown in **a**, **c**, **d**, **e**, **g** and **h** were analysed with the two-tailed Wilcoxon signed-rank test. Data shown in **b**, **f** and **i** were analysed with the two-tailed Spearman correlation test. Horizontal and vertical bars denote mean and standard deviation, respectively.

immunization (Extended Data Fig. 3h,i) and at 2 weeks (week 14) following the last immunization ($P < 0.0001$ for both timepoints; Fig. 2g,h). The vaccine-induced capacity of CD14+ cells to engulf apoptotic cells following in vitro SAMT-247 treatment trended with a reduced risk of viral acquisition in the animals treated in vivo with SAMT-247 ($R = 0.42$, $P = 0.065$; Fig. 2i).

These data support the hypothesis that SAMT-247 synergizes with vaccine-induced responses at multiple levels: increasing NKG2A+ cytotoxic function and V2-specific protective ADCC and enhancing

the functionality of protective NKp44+ cells and CD14+ cells (essential responses to maintain tissue homeostasis and curb inflammation (Extended Data Table 1a).

SAMT-247 modulates IL-10, IFN-γ and TNF-α expression in CD4+ T cells
Vaccine-induced gut homing-activated $α_4β_7^+CD4^+$ T cells expressing the SIV/HIV co-receptor CCR5 ($α_4β_7^+CCR5^+CD4^+$ cells) have been associated with an increased risk of virus acquisition[33,34]. Here we found
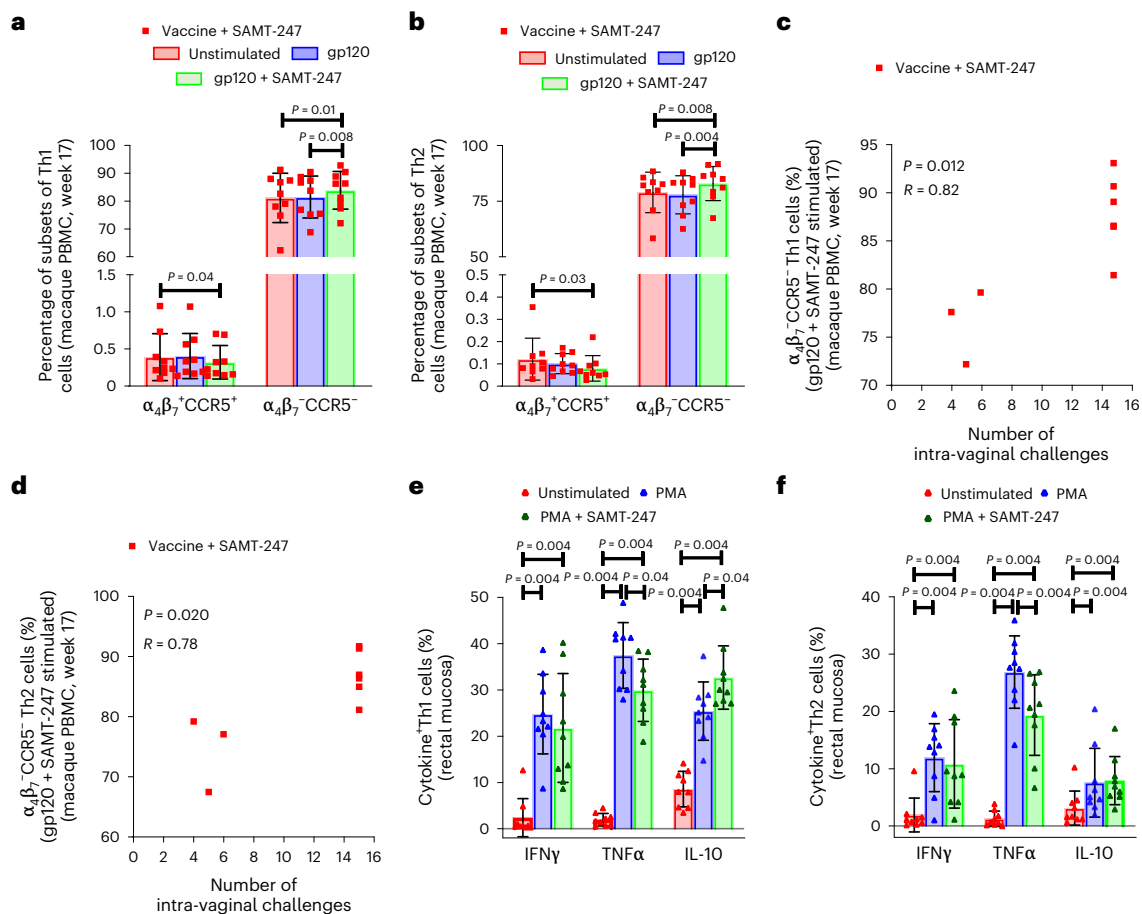
Fig. 3 | T-cell responses ex vivo and in vitro. a,b, Evaluation of CCR5 and $\alpha_4\beta_7$ markers on Th1 and Th2 cells in the absence or presence of stimuli in the vaccine + SAMT-247 group animals ($n = 9$). **c,d,** Correlation of gp120 peptide + SAMT-247 stimulated CCR5$^-\alpha_4\beta_7^-$ Th1 ($P = 0.012$) and Th2 cells ($P = 0.020$) with number of intravaginal challenges in the vaccine + SAMT-247 group ($n = 9$). **e,f,** IFN-γ^+, TNF-α^+ and IL-10$^+$ Th1 and Th2 cells in the rectal mucosa in the absence or presence of stimuli ($n = 9$). Data shown in **a**, **b**, **e** and **f** were analysed with the two-tailed Wilcoxon signed-rank test. Data shown in **c** and **d** were analysed with the two-tailed Spearman correlation test. Horizontal and vertical bars denote mean and standard deviation, respectively.

that vaccination with the ΔV1DNA/ALVAC/ΔV1gp120/alum regimen decreased the frequency of vaccine-induced (Ki67$^+$) $\alpha_4\beta_7^+$CCR5$^+$ memory Th1 (CD4$^+\alpha_4\beta_7^+$CCR5$^+$CCR6$^-$CXCR3$^+$Ki67$^+$CD95$^+$) and to a lesser extent Th2 (CD4$^+\alpha_4\beta_7^+$CCR5$^+$CCR6$^-$CXCR3$^-$Ki67$^+$CD95$^+$) cell phenotypes ($P < 0.0001$ and $P = 0.01$, respectively), and significantly increased the frequency of $\alpha_4\beta_7^-$CCR5$^-$CD4$^+$ memory Th1 and Th2 cells in all vaccinated macaques ($P < 0.0001$ for both; Extended Data Fig. 4a–e). To assess the effect of virus acquisition on the activation status of CD4$^+$ T cells, we stimulated cryopreserved ex vivo PBMCs from vaccinated animals (week 17) with overlapping peptides encompassing the entire gp120 envelope protein to simulate host response at the time of virus encounter in the presence or absence of SAMT-247. SAMT-247 + gp120 peptides decreased the frequency of vaccine-induced (Ki67$^+$) $\alpha_4\beta_7^+$CCR5$^+$ Th1 and Th2 cells ($P = 0.04$ and $P = 0.03$, respectively; Fig. 3a,b) and increased $\alpha_4\beta_7^-$CCR5$^-$ Th1 and Th2 cells ($P = 0.008$ and $P = 0.004$, respectively; Fig. 3a,b). Strikingly, at week 17 the percentage of both $\alpha_4\beta_7^-$CCR5$^-$ Th1 and Th2 cells following in vitro stimulation with gp120 and SAMT-247 significantly correlated with delayed virus acquisition in vivo ($R = 0.82$, P = 0.012 and $R = 0.76$, $P = 0.020$, respectively; Fig. 3c,d). At the same timepoint (week 17), we assessed whether SAMT-247 affected expression of T-cell activation/proliferation/exhaustion on molecules positively and negatively associated with immune responses. This included the receptors/ligand markers OX40, expressed on activated T cells[35], CD40 ligand (CD154), which triggers a short-term CD4$^+$ T-cell activation response[36], early activation marker CD69 (ref. [37]),

and proliferation marker ki67 (ref. [38]). We additionally evaluated the negative regulators CTLA-4 and PD-1, which inhibit T-cell activation[39], the PD-L1/PD-1 pathway, which contributes to T-cell exhaustion[40], and the exhaustion marker Lag-3 (ref. [41]). SAMT-247 did not augment gp120 modulation of any one of these molecules (Extended Data Figs. 5 and 6).

Next, we investigated the effect of SAMT-247 treatment on mucosal Th1 and Th2 cells of age-matched macaques following PMA stimulation. While the overall mucosal Th1 and Th2 cell frequencies did not change upon PMA stimulation (Extended Data Fig. 7a,b), SAMT-247 treatment was associated with a significant decrease in TNF-α production in Th2 cells and more weakly in Th1 cells ($P = 0.004$ and $P = 0.04$, respectively) as well as with increased IL-10 production in Th1 cells ($P = 0.04$; Fig. 3e,f and Extended Data Table 1b).

Zinc availability and SAMT-247 function
The spectrum of SAMT-247 effects on NK cell, monocyte and T-cell functions described above suggested that SAMT-247 may affect a central component of immunity. Since zinc is a master regulator of immunity[42,43], we hypothesized that SAMT-247 may have augmented vaccine-induced immunity by ejecting zinc from proteins and affecting its distribution in immune cells. We used confocal microscopy to measure cellular zinc in human NK cells stimulated with PMA with or without SAMT-247 in the presence or absence of a zinc chelator. PMA + SAMT-247-treated cells had significantly brighter zinc staining per cell compared with unstimulated ($P = 0.04$) and a trend with
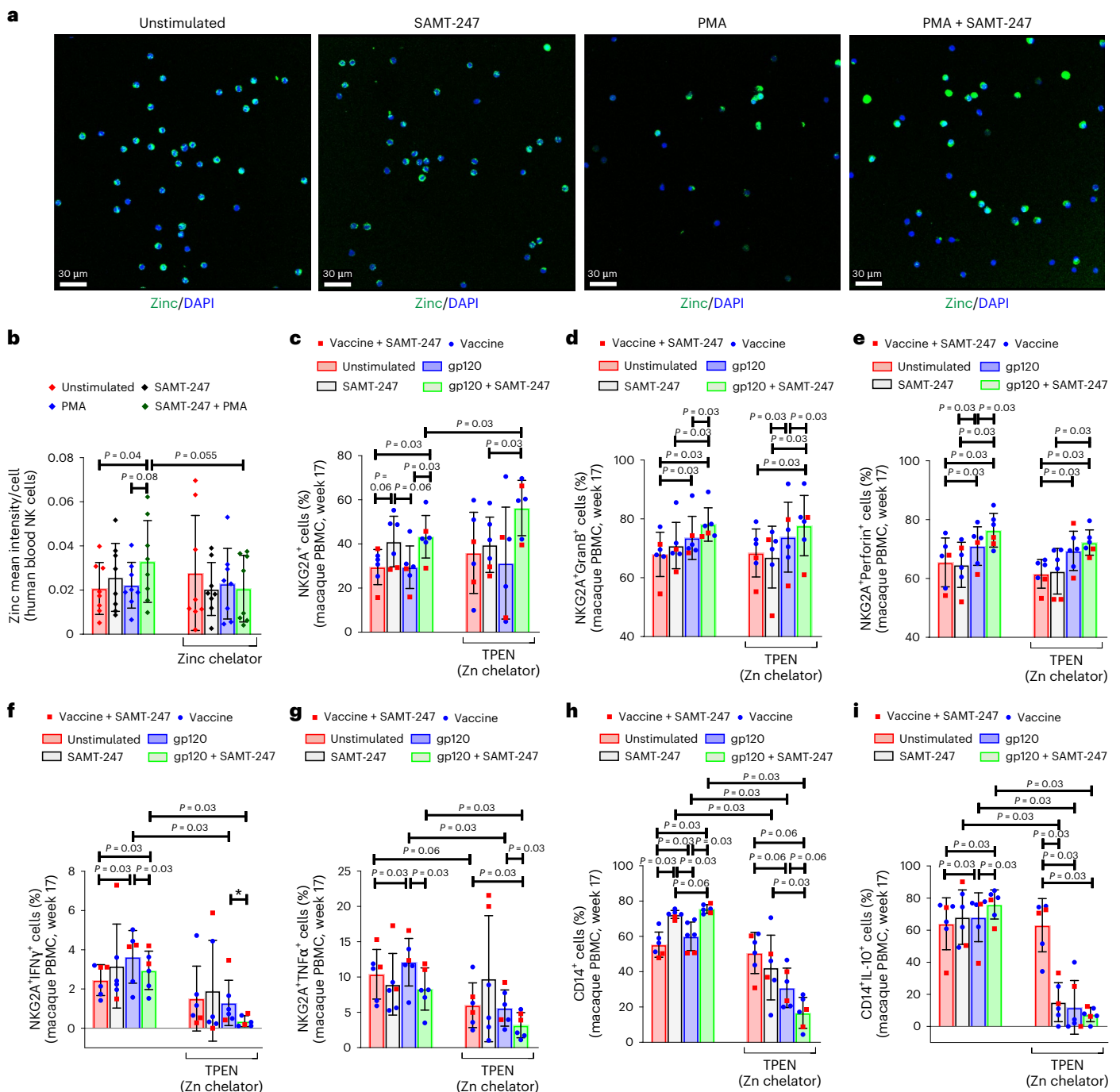
**Fig. 4 | Effect of zinc chelation on NK and monocyte functions.**
a, Representative imaging of human NKG2A+ cells unstimulated or stimulated with SAMT-247, PMA or PMA + SAMT-247. **b**, Mean zinc intensity in NKG2A+ cells of the healthy human donor in the presence or absence of zinc chelator in different stimulation conditions ($n = 8$). Fluorescence intensity of each field was measured for zinc expression as indicated by green colour, and the total number of DAPI positive cells were counted to determine the mean intensity of zinc/ cells using iMARIS software. The mean of two duplicate fields was evaluated for the calculation. **c**, Comparison of expressions of NKG2A marker in macaques in the absence or presence of zinc chelator and stimuli in the vaccine + SAMT- 247 group ($n = 4$) and vaccine group ($n = 2$). **d–g**, Comparison of expressions of granzyme B, perforin, IFN-γ and TNF-α by macaque blood NKG2A+ cells from week 17 in the absence or presence of different stimulations and zinc chelator in the vaccine + SAMT-247 group ($n = 4$) and vaccine group ($n = 2$). **h,i**, Evaluation of the frequency of CD14+ monocytes and CD14+IL-10+ monocytes in the absence or presence of zinc chelator and stimuli in the vaccine + SAMT-247 group ($n = 4$) and vaccine group ($n = 2$). Data shown in **b–i** were analysed with the two-tailed Wilcoxon signed-rank test. Horizontal and vertical bars denote mean and standard deviation, respectively.

PMA-stimulated cells ($P = 0.08$; Fig. 4a,b), which trended for a decrease in the presence of the zinc chelator ($P = 0.055$; Fig. 4b).

Next, we investigated the contribution of divalent free zinc to the protective immune responses using cryopreserved ex vivo PBMCs from vaccinated macaques (week 17). To mimic virus exposure, we stimulated cells in vitro with SIV gp120 envelope peptides in the presence or absence of SAMT-247 and of the membrane-permeable intracellular zinc chelator N,N,N',N' tetrakis-(2-pyridyl-methyl) ethylendiamine (TPEN). Zinc chelation did not affect either SAMT-247-associated NKG2A+ survival nor their ability to increase granzyme B and perforin
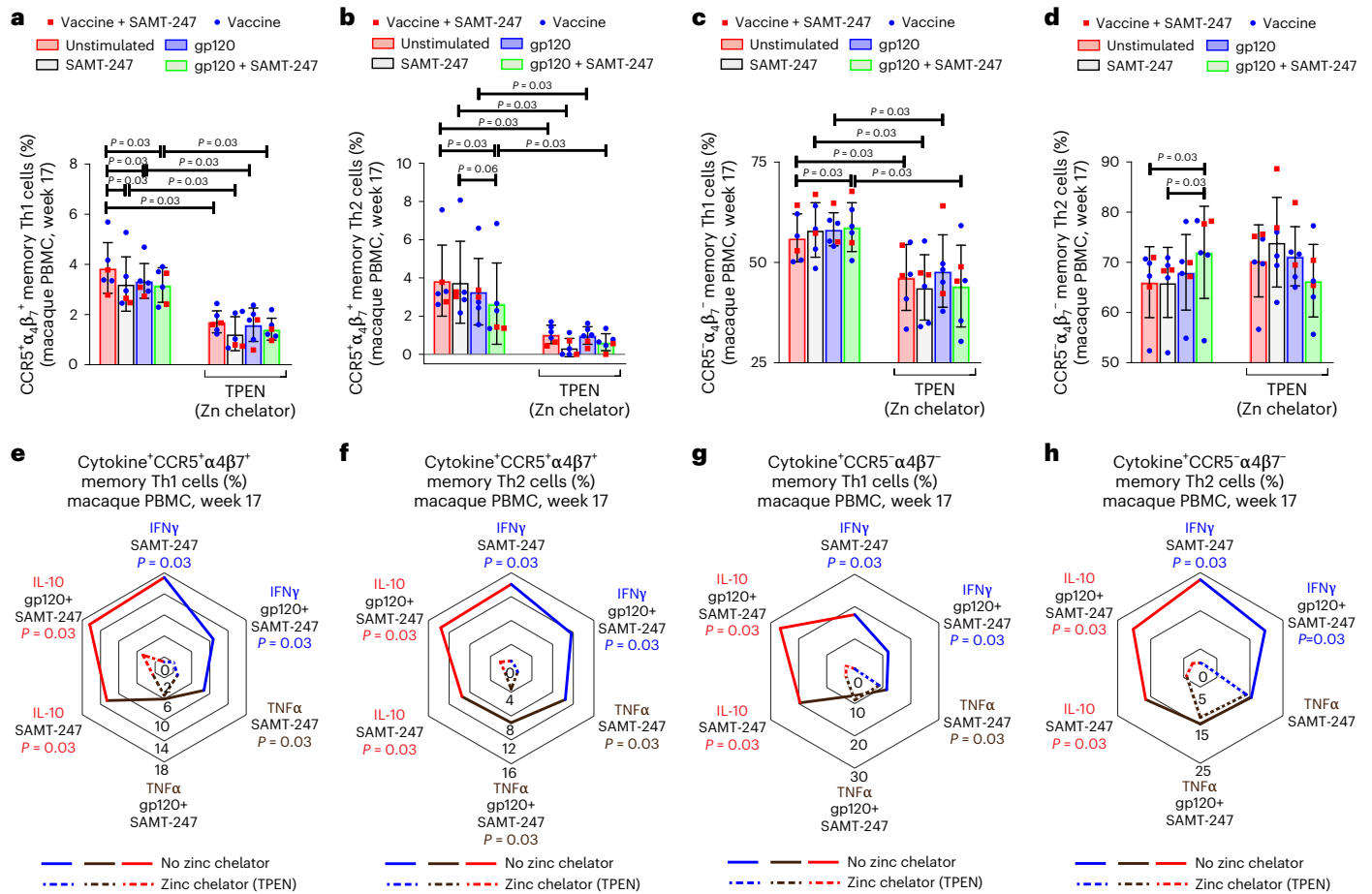
Fig. 5 | Effect of zinc chelation on CCR5$^{+/-}$ and α$_4$β$_7$$^{+/-}$ Th1 and Th2 cells.
a–d, Comparison of expressions of CCR5 and α$_4$β$_7$ markers in Th1 and Th2 memory cells in the absence or presence of zinc chelator and stimuli in the vaccine+SAMT-247 group ($n = 4$) and vaccine group ($n = 2$). **e–h**, Radar plots comparing different expressions of cytokines by different subsets of Th1 and Th2 cells from vaccinated animals at week 17 in the absence or presence of stimulation and zinc chelator ($n = 6$). Data shown in **a–h** were analysed with the two-tailed Wilcoxon signed-rank test. Horizontal and vertical bars denote mean and standard deviation. The radar plot represents the mean percentage value of cytokine responses. Solid lines represent the absence of zinc chelator and dashed lines represent the presence of zinc chelator.

following gp120 peptide stimulation, suggesting that these SAMT-247 activities are not dependent on zinc (Fig. 4c–e). In contrast, TPEN treatment significantly decreased both IFN-γ and TNF-α expression following gp120 peptide or gp120 peptide/SAMT-247 stimulation, suggesting that, by ejecting zinc, SAMT-247 may affect the structural stability of transcription factors for cytokines, and further, that TPEN treatment exacerbates this effect by removing zinc from proteins and sequestering intracellular divalent zinc (Fig. 4f,g). This hypothesis is supported by similar results obtained using human NKG2A$^+$ cells (Extended Data Fig. 7c–g).

Several monocyte functions such as monocyte and macrophage phagocytosis are dependent on zinc and can be restored via supplements. Recent studies in humans also demonstrate that the level of intracellular zinc correlates with efferocytosis, itself induced by pro-resolution IL-10 via an IL-10-mediated endocrine mechanism[44–46]. We therefore assessed the effect of zinc chelation on SAMT-247-associated CD14$^+$ cell function by stimulating cryopreserved ex vivo CD14$^+$ cells from vaccinated animals (pre-immunization and week 13) with gp120 pooled peptides in the presence or absence of SAMT-247 and TPEN. We observed an increased percentage of CD14$^+$ cells following SAMT-247 treatment ($P = 0.03$; Fig. 4h), suggesting increased survival of this cell subset in the presence of the drug. However, the frequency of CD14$^+$ cells as well as their ability to produce IL-10

greatly diminished following TPEN treatment (Fig. 4i). These data are consistent with prior work demonstrating that divalent zinc increases the survival and functionality of CD14$^+$ cells[47].

Lastly, we assessed the effect of zinc chelation on cryopreserved ex vivo CCR5 and α$_4$β$_7$ positive or negative Th1 and Th2 elicited by vaccination (week 17). PBMCs were stimulated with gp120 pooled peptides in the presence or absence of SAMT-247 and TPEN. Zinc chelation resulted in a dramatic decrease of CCR5$^+$ α$_4$β$_7$$^+$ CD4$^+$ Th1 and Th2 subsets in all conditions (Fig. 5a,b). TPEN caused a significant decrease in the percentage of Th1 negative for CCR5 and α$_4$β$_7$ expression ($P = 0.03$ for all conditions; Fig. 5c), but did not affect the percentage of Th2 cells negative for CCR5 and α$_4$β$_7$ expression (Fig. 5d). The expression of IFN-γ, TNF-α and IL-10 was significantly compromised by zinc chelation in Th1 and Th2 cells in most stimulation conditions, regardless of their expression of CCR5 and α$_4$β$_7$ (Fig. 5e–h and Extended Data Figs. 8 and 9). TNF-α expression in CCR5 and α$_4$β$_7$ negative Th1 and Th2, however, was not affected with the same severity (Extended Data Figs. 8 and 9).

Collectively, these data demonstrate differential susceptibility of Th1 and Th2 to SAMT-247 and differential dependence on zinc. SAMT-247 in the presence of gp120 peptide increases the viability of Th2 negative for CCR5 and α$_4$β$_7$ expression and increases expression of IL-10 in all Th1 and Th2 subsets, probably creating an anti-inflammatory
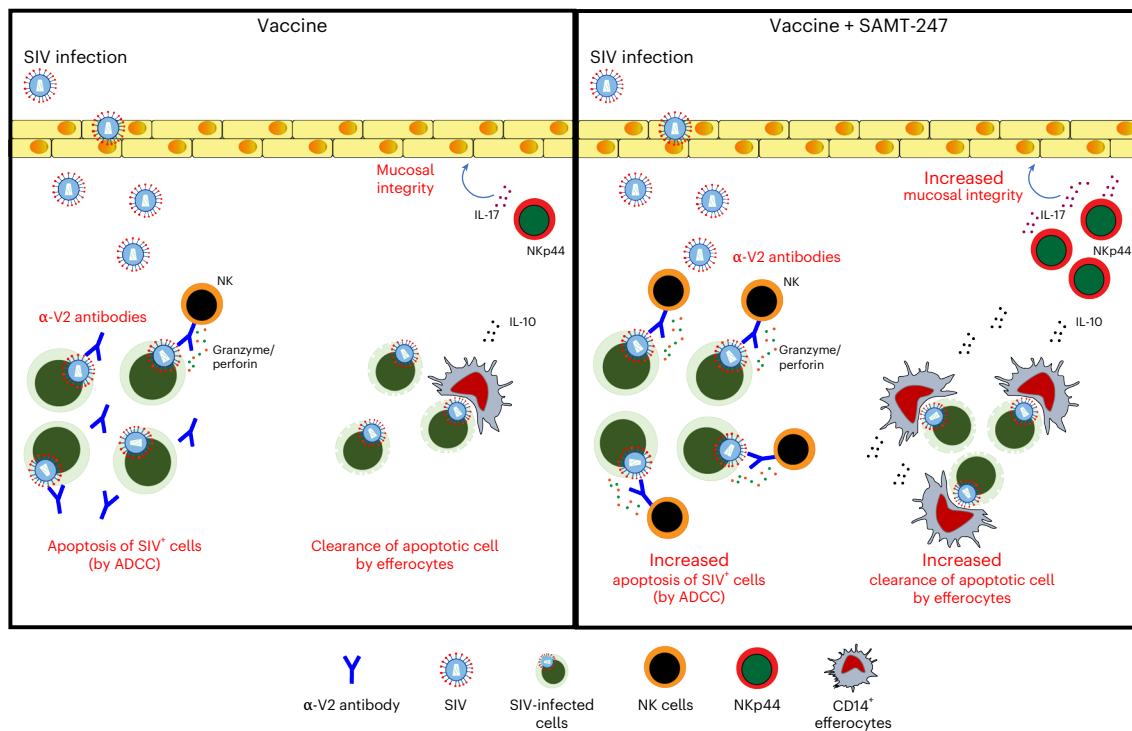
Fig. 6 | Model for SAMT-247 modulation of mucosal immune responses. Vaccination-induced ADCC results in apoptosis of SIV-infected cells, which in turn are cleared by efferocytes to avoid inflammation and preserve tissue homeostasis. Vaccine-induced IL-10 expression in CD14^{+} monocytes further augments efferocytosis. Vaccine-induced NKp44^{+} cells produce the IL-17 cytokine that maintains mucosal epithelium integrity. All of these protective effector responses were enhanced dramatically in the vaccine + SAMT-247 group, increasing protection from SIV$_{mac251}$ acquisition. The scheme is adapted from Bissa et al.[15].

environment. IL-10 production is inhibited by zinc chelation; IFN-γ production is highly dependent on zinc in all Th1 and Th2 cell subsets, whereas the decrease in TNF-α expression mediated by SAMT-247 appears to be less zinc dependent (Extended Data Table 1c).

Discussion

In this pre-clinical macaque study, we investigated whether topical administration of gel-formulated S-acyl-2 mercaptobenzamide thioester SAMT-247, which inhibits in vitro HIV maturation and infectivity[48,49], synergized with DNA/ALVAC/gp120/alum vaccination. As previously reported[15,16], vaccination alone decreased the risk of SIV$_{mac251}$ acquisition by 65%, and SAMT-247 treatment alone, given 4 h before challenge exposure, had no effect. However, topical SAMT-247 treatment of vaccinated females resulted in a striking 92.7% reduction of per-challenge risk of SIV$_{mac251}$ acquisition, suggesting SAMT-247 additional effects, other than its virucidal activity. We hypothesized that SAMT-247 affected immunity. Using plasma or ex vivo cryopreserved cells from vaccinated animals, respectively, we demonstrated in vitro that SAMT-247 augments NKG2A-mediated ADCC, monocyte efferocytosis and IL-10 production.

Strikingly, SAMT-247 treatment in vitro, also reduced expression of IFN-γ, pro-inflammatory cytokine TNF-α, and CCR5 expression in ex vivo cryopreserved T cells from vaccinated animals, thereby decreasing target cells for SIV infection. Lastly, we demonstrated that in vitro treatment of rectal mucosal cells from macaques increased the frequency of mucosal IL-17-producing NKp44 cells. All of these immune responses have been shown to reproducibly correlate with reduced risk of virus acquisition in vaccinated animals[13–16,23]. Taken together, these findings suggest that SAMT-247's ability to eject zinc from transcription factors or enzymes may enable zinc-mediated vaccine-induced immunity and protection.

Zinc is an essential micronutrient and is a structural constituent in approximately 800 zinc-finger transcription factors[50] and 2,000 enzymes[51]. Its role in immunity is well known[42,43,52,53]. Relevant to the vaccine approach tested here, zinc and zinc transporters have a role in efferocytosis[46] and zinc supplementation augments granulocyte and monocyte phagocytic function[54]. Intracellular zinc mobilization is triggered by the activation of the c-AMP pathway in human pathogens[55], and a dysfunction of Th2 responses linked to defective reprogramming of monocytes to anti-inflammatory M2 macrophages has been demonstrated in mice fed a zinc-deficient diet[56]. Indeed, we found that in vitro chelation of zinc by TPEN affected SAMT-247 modulation of IFN-γ, TNF-α and CCR5 expression in stimulated T cells, as well as IL-10 in monocytes. In contrast, zinc chelation did not affect the SAMT-247-associated increase of perforin and granzyme in NK cells (Extended Data Table 1c). Therefore, we conclude that SAMT-247 synergizes with the DNA/ALVAC/gp120/alum vaccine regimen as an immune enhancer by augmenting the immunological function of effector cells (Fig. 6).

We cannot however exclude a possible contribution of the anti-viral effect of SAMT-247 in reducing virus infectivity in the vaginal mucosa. In our study, we did not observe an effect on virus acquisition by SAMT-247 alone in naïve animals, though it must be noted that the protective effect of SAMT-247 alone previously reported in the SIV$_{mac251}$ model was obtained in animals mock-immunized with empty Ad vector and, relevant to the alum adjuvant[31], a key contributor to the immunological landscape created by the DNA/ALVAC/gp120/alum vaccine.

In summary, we provide evidence that a combination of the V1-deleted envelope virus-like particle delivered with the DNA/ALVAC/gp120/alum vaccine platform, and SAMT-247 is highly efficacious in preventing vaginal infection by a neutralization-resistant, highly pathogenic virus. Our data also suggest that ADCC and efferocytosis may be

true effectors of protection against SIV/HIV, pointing to an underestimated role of monocytes and NK cells in vaccine efficacy. Finally, our data underscore the importance of pro-resolution anti-inflammatory responses able to maintain low levels of T-cell activation in protection from SIV/HIV acquisition.

Methods

This research complies with all relevant ethical regulations. The NCI Animal Care and Use Committee (ACUC) approved the vaccine study. Nine additional animal tissues were obtained from our collaborative study with the Tulane animal facility, and the study was approved by the Tulane ACUC. Human PBMCs were obtained from eight healthy donors via an institutional review board-approved National Institutes of Health (NIH) protocol.

Animals

Fifty female Indian rhesus macaques obtained from the free-range breeding colony on Morgan Island, South Carolina, were used in this study. The macaques, aged 2–3 years at study initiation, were negative for SIV, simian retrovirus and Simian T-Cell Leukemia Virus (STLV), and were MHC typed for Mamu A*01, Mamu B*17 and Mamu B*08. The macaques were randomized by the statistician on the basis of age, weight and haplotype before being divided into four groups: vaccine/microbicide group (20 macaques, 3 A*01 positive, 1 B*17 positive and 1 B*08 positive); vaccine-only group (18 macaques, 3 A*01 positive and 1 B*17 positive); microbicide-only group (6 macaques, 1 both A*01 positive and B*17 positive) and control group (6 macaques, 1 both A*01 positive and B*17 positive). These group sizes were determined on the basis of a previous vaccine study comparing 14 vaccinated macaques and 18 controls[15,16], and on a pilot experiment in which we defined a time between microbicide administration and viral challenge that would decrease the microbicide efficacy so that we could observe an additive/synergistic effect[31]. We selected a 4 h 'window' between administration of microbicide and viral challenge, as this time frame was demonstrated ineffective with SAMT-247 alone[31]. The historical control macaques and microbicide macaques were also used in the statistical analysis. Infection rates were assumed to equal those of the previously observed gel-only and microbicide groups, 0.333 and 0.133, respectively, and the vaccine and combination groups, 0.120 and 0.040. The treatment efficacies of the latter three groups relative to the gel-only group were expected to be 60% (microbicide), 64% (vaccine) and 88% (combination). When the animals were given up to 14 viral challenges and the number of challenges to infect the animals was compared using the Wald test of the proportional hazards model with all four groups analysed together, then the power of the test at the two-sided 0.05 level between the vaccine group and the combination group was expected to be 79%, while the comparisons of these two groups individually versus the control group would respectively have 82% and 99% power. The test of the microbicide group versus the combination group would have 63% power. Data on 31 historical naïve controls intravaginally challenged with the same dose and lot of SIV$_{mac251}$ were added to the control group to increase statistical power. There was no difference between the concurrent and historical controls in rate of SIV acquisition ($P = 0.74$). Macaques were housed and maintained at the NCI Animal Facility at the NIH, Bethesda, MD. All animals were handled in accordance with the standards of the Association for the Assessment and Accreditation of Laboratory Animal Care (AAALAC) in an AAALAC-accredited facility (OLAW, Animal Welfare Assurance A4149-01 for NIH). All animal care and procedures were carried out under protocols approved by the NCI ACUC before study initiation. Animals were closely monitored daily for any signs of illness, and appropriate medical care was provided as needed. Animals were socially housed per the approved ACUC protocol and social compatibility except during the viral challenge phase when they were individually housed. All clinical procedures, including biopsy collection, administration of anaesthetics and analgesics, and euthanasia, were carried out under the direction of a laboratory animal veterinarian. Steps were taken to ensure the welfare of the animals and minimize discomfort of all animals used in this study. Animals were fed daily with a fresh diet of primate biscuits, fruit, peanuts and other food items to maintain body weight or normal growth. Animals were monitored for psychological wellbeing and provided with physical enrichment including sanitized toys, destructible enrichment (cardboard and other paper products) and audio and visual stimulation.

Additionally, rectal tissue from nine random female rhesus macaques aged 2–3 years was used for an in vitro study. The age-matched macaques from this separate study included four animals vaccinated against HIV and five naïve animals, all challenged with Simian-human immunodeficiency viruses (SHIV). Rectal tissue was obtained post challenge from seven infected and two uninfected animals for the analysis of this study. Extra cells were available from that collection and were used here for the in vitro study. Macaques were housed and maintained at the Tulane University animal facility. The nine animals were handled in accordance with the standards of the Association for the Assessment and Accreditation of Laboratory Animal Care in an AAALAC-accredited facility (OLAW, Animal Welfare Assurance). The care of the nine animals and all procedures were carried out under protocols approved by the Tulane ACUC.

Human healthy volunteers

Human PBMCs were obtained from eight healthy donors on an institutional review board-approved NIH protocol (99-CC-0168). Research blood donors provided written informed consent and blood samples were de-identified before distribution. Clinical Trial Number: NCT00001846.

Immunization and challenge

Macaques in the vaccine/microbicide and vaccine-only groups were immunized at weeks 0 and 4 with DNA encoding SIVgp160ΔV1 (2 mg per dose) and SIV239gag (1 mg per dose) in a total volume of 1 ml PBS. The DNA was administered in both thighs (0.5 ml to each). At 8 weeks the macaques were administered ALVAC encoding *gag/pro/env* (wild-type *env*) in the right thigh, 10^8 pfu per dose in 1 ml PBS. At week 12 the macaques were boosted with the same ALVAC plus SIVgp120ΔV1 protein (400 µg per dose in 500 µl PBS plus 500 µl 2% Alhydrogel). The ALVAC was administered to the right thigh; the 1 ml dose of Env protein plus alum was administered to the left thigh. Beginning at week 17 all macaques were challenged intravaginally weekly with 1 ml of a SIV$_{mac251}$ stock containing 4000 TCID$_{50}$/mL (evaluated in rhesus 221 cells). Up to 14 challenges were administered until the macaques became SIV positive as assessed by droplet digital PCR (H. K. Chung, J. Narola, H. Babbar, M. Naseri, N. Richardson, R. Pal and T. Fouts, manuscript in preparation). Doses of 2 ml of the microbicide, SAMT-247, were administered as a gel intravaginally to macaques in the vaccine/microbicide group and the microbicide-only group 4 h before each SIV challenge. The 2 ml gel contained 0.8% SAMT-247 in HEC gel (2.7% Natrosol cellulose 250HX Pharma, 0.01% DMSO and 0.9% saline). Macaques in the vaccine-only group and control group received HEC gel lacking only the SAMT-247. Rhesus macaques were vaccinated and samples were collected during the vaccination period as well as following vaginal exposure of the animals to SIV$_{mac251}$. The same material cannot be obtained multiple times from the same monkey, making these biological specimens unique.

IgG plasma titres to gp120

gp120 total IgG antibodies were measured by ELISA. ELISA plates (Nunc Maxisorp 96-well plate) were coated with 100 µl of 500 ng ml^{-1} SIV$_{mac251-M766}$ gp120 protein per well in 50 mM sodium bicarbonate buffer pH 9.6 and incubated overnight at 4 °C. Plates were blocked with 200 µl PBS Superblock (Thermo Fisher Scientific) for 1 h at room temperature. Plasma samples were serial-diluted with sample diluent (Avioq), and 100 µl of

diluted plasma was added to the wells. Plates were covered and incubated for 1 h at 37 °C, washed six times with PBS Tween 20 (0.05%) and incubated with 100 μl of anti-human HRP diluted at 1:120,000 in sample diluent (Avioq) for 1 h covered at 37 °C. The plates were washed six times. Plates were developed using 100 μl K-Blue Aqueous substrate (Neogen) to all wells and incubated for 30 min at room temperature. The reaction was stopped by the addition of 100 μl of 2 N sulfuric acid to all wells and the plate was read at 450 nm on a Molecular Devices E-max plate reader.

Pepscan

Plasma samples were assayed by PEPSCAN analysis using SIV$_{mac251}$ gp120 linear peptides[16]. ELISA plates (Nunc Maxisorp) were coated with 100 ng of each of the 1–89 overlapping peptides (with 15 amino acids each encompassing the entire SIV$_{mac251}$ gp120 sequence) in 50 mM NaHCO3, pH 9.6, per well, incubated overnight at 4 °C, and blocked with 200 μl of Pierce SuperBlock blocking buffer in PBS for 1 h at room temperature. Serum samples were diluted at 1:50 in sample diluent (Avioq), and 100 μl were added to the plate and incubated for 1 h at 37 °C. Plates were washed six times with PBS Tween 20 (0.05%) and incubated with 100 μl anti-human HRP diluted at 1:120,000 in sample diluent (Avioq) to all wells and incubated, covered, for 1 h at 37 °C. The plates were again washed six times and developed using 100 μl of K-Blue Aqueous substrate (Neogen) to all wells and incubated 30 min at room temperature. The reaction was stopped by adding 100 μl of 2 N sulfuric acid to all wells and plate was read at 450 nm on a Molecular Devices E-max plate reader.

Rectal mucosal NK/ILC phenotyping and cytokine expression upon gp120 peptides/PMA-Ionomycin stimulation in vaccinated animals

The frequency and cytokine levels of NK/ILCs were measured in macaque rectal mucosa pre-vaccination and 1 week post last vaccination (week 13). Freshly collected rectal biopsies were treated with collagenase (2 mg ml^{-1}; Sigma-Aldrich) in the absence of FBS in 37 °C for 1 h, then mechanically separated by using a 10 ml syringe with a blunt head canula. Biopsies were washed with R10 and passed through a 70 μm cell strainer. Single cells were counted and used for the experiment[23]. A portion of the cells were phenotyped and the rest were cultured in R10 in the presence/or absence of gp120 peptides or PMA (phorbol 12-myristate 13-acetate)-Ionomycin for 12 h. Subsequently, cells were stained with Live/Dead Aqua Dye (cat. no. L34966, 0.5 μl) from Thermo Fisher, followed by surface staining with the following: Alexa 700 anti-CD3 (SP34-2; cat. no. 557917, 5 μl), Alexa 700 anti-CD20 (2H7; cat. no. 560631, 5 μl), Alexa 700 anti-CD11b (ICRF44; cat. no. 557918, 5 μl), APC-Cy7 anti-CD16 (3G8; cat. no. 557758, 5 μl), PE-CF594 anti-CD56 (B159; cat. no. 562289, 5 μl) BV650 anti-NKp44 (P44-8; cat. no. 744302, 5 μl), BV786 anti-CD45 (D058-1283; cat. no. 563861, 5 μl) from BD Biosciences; and PE-Cy7 anti-NKG2A (Z199; cat. no. B10246, 5 μl) from Beckman Coulter for 30 min at room temperature. This was followed by permeabilization with a FOXP3-transcription buffer set (cat. no. 00−5523-00) from eBioscience according to the manufacturer's recommendation and subsequently intracellular staining with the following: BV421 anti-IFN-γ (B27; cat. no. 562988, 5 μl) from BD Biosciences and PE-Cy5.5 anti-IL-17 (BL168; cat. no. 512314, 5 μl) from BioLegend for 30 min at room temperature. Samples were acquired on a BD FACSymphony A5 cytometer and analysed with FlowJo software 10.6. NKG2A$^+$ NK cells were gated as singlets, live cells, CD45$^+$ cells, CD3$^-$, CD20$^-$, CD11b$^-$ and NKG2A$^+$ NKp44$^-$ cells. NKp44$^+$ cells were gated as singlets, live cells, CD45$^+$ cells, CD3$^-$, CD20$^-$, CD11b$^-$ and NKG2A$^-$ NKp44$^+$ cells. NKG2A$^-$ NKp44$^-$ cells were gated as singlets, live cells, CD45$^+$ cells, CD3$^-$, CD20$^-$, CD11b$^-$ and NKG2A$^-$ NKp44$^-$ cells. Cytokines were gated on parent population.

CD4$^+$ T-cell phenotypes

The levels of CD4$^+$ T-cell subsets were measured in blood at baseline and week 13 in vaccinated animals. PBMCs were stained with the following: LIVE/DEAD Fixable Blue Dead Cell Stain (cat. no. L23105, Thermo Fisher); Alexa 700 anti-CD3 (SP34-2; cat. no. 557917, 5 μl), BV785 anti-CD4 (L200; cat. no. 563914, 5 μl), PeCy5 anti-CD95 (DX2; cat. no. 559773, 5 μl), BV650 anti-CCR5 (3A9; cat. no. 564999, 5 μl), BUV496 anti-CD8 (RPA-T8; cat. no. 564804, 5 μl), BUV737 anti-CD28 (CD28.2; cat. no. 612815, 5 μl) and FITC anti-Ki67 (B56; cat. no. 556026, 5 μl) from BD Biosciences; APC Cy7 anti-CXCR3 (G025H7; cat. no. 353722, 5 μl), BV605 anti-CCR6 (G034E3; cat. no. 353420, 5 μl), BV510 anti-CD127 (A019D5; cat. no. 351332, 5 μl), BV750 anti-PD-1 (EH12.2H7; cat. no. 329965, 5 μl) and BV711 anti-CD25 (BC96; cat. no. 302636, 5 μl) from BioLegend; PE-eFluor 610 anti-CXCR5 (MU5UBEE; cat. no. 61-9185-42, 5 μl), eFluor 450 anti-FoxP3 (236A/E7; cat. no. 48-4777-42, 5 μl) from eBioscience; and APC anti-α$_4$β$_7$, provided by the NIH Nonhuman Primate Reagent Resource (R24 OD010976, and NIAID contract HHSN272201300031C). Samples were acquired on a BD FACSymphony A5 cytometer and analysed with FlowJo software 10.6. Gating was done on live CD3$^+$CD4$^+$ cells and on vaccine induced Ki67$^+$ cells. CXCR3 and CCR6 expression were used to identify Th1 or Th2 populations[14].

ADCC CEM-based assay

ADCC activity was assessed using EGFP-CEM-NKr-CCR5-SNAP cells that constitutively express GFP as targets[23,57]. Briefly, one million target cells were incubated with 50 μg of ΔV1 gp120 protein for 2 h at 37 °C. After this coating, the target cells were washed and labelled with SNAP-Surface Alexa Fluor 647 (New England Biolabs) per manufacturer recommendations for 30 min at room temperature. Plasma samples, heat inactivated at 56 °C for 30 min, were serially diluted (seven ten-fold dilutions starting at 1:10) and 100 μl were added to wells of a 96-well V-bottom plate (Millipore Sigma). A total of 5,000 target cells (50 μl) and 250,000 human PBMCs (50 μl) were added as effectors to each well to give an effector/target (E/T) ratio of 50:1. The plate was incubated at 37 °C for 2 h followed by two PBS washes. The cells were resuspended in 200 μl of a 2% PBS−paraformaldehyde solution and acquired on a Symphony equipped with a high-throughput system (BD Biosciences). Specific ADCC activity was measured by loss of GFP from the SNAP-Surface Alexa647$^+$ target cells. Target and effector cells cultured in the presence of R10 medium were used as background. Anti-SIVmac gp120 monoclonal antibody KK17 (NIH AIDS Reagent Program) was used as a positive control. Normalized ADCC activity was calculated as: (ADCC activity in the presence of plasma − background)/(ADCC activity in the presence of KK17 − background) × 100. The normalization was done to minimize plate-to-plate and experiment-to-experiment variation of the assay. The ADCC endpoint titre is defined as the reciprocal dilution at which the percent ADCC activity was greater than the mean percent ADCC activity of the background wells containing medium only with target and effector cells, plus three standard deviations.

Inhibition of ADCC CEM-based assay by monoclonal F(ab')2 of NCI05 and NCI09

F(ab')2 fragments were prepared from both NCI05 or NCI09 mAb, as these antibodies recognize overlapping conformationally distinct V2 epitopes[16], using Pierce F(ab')2 Micro Preparation Kit (cat. no. 44688, Thermo Fisher) following the manufacturer's instructions. An SDS−PAGE gel with the recovered F(ab')2 was run and Silver stained (cat. no. LC6070, Silver Quest staining Kit, Invitrogen) according to the manufacturer's instructions, to assure the purity of the F(ab')2 fragments. Target cells, coated with ΔV1 gp120 protein as indicated above and labelled with SNAP-Surface Alexa Fluor 647, were incubated for 1 h at 37 °C with 5 μg ml^{-1} of purified F(ab')2 fragments from NCI05, or NCI09 monoclonal antibodies. Cells incubated without F(ab')2 served as control. These target cells were subsequently used in the ADCC assay as described above. These F(ab')2 inhibit binding (and ADCC) mediated by the anti-V2 antibodies from immunized animals' plasma. The percentage ADCC activity difference in the presence or absence of F(ab')2 is considered V2-specific ADCC activity.

ADCC assay using SAMT-247

Ten million human PBMC effector cells were resuspended in 1 ml of R10 medium and incubated in the presence/absence of 100 μM of SAMT-247 for 4 h. Cells were washed and used as effector cells to measure ADCC activity as described above. SAMT-247-induced ADCC was measured by subtracting ADCC without SAMT-247-treated effector cells from ADCC with SAMT-247-treated effector cells.

Efferocytosis assay

The frequency of efferocytotic CD14+ cells was assessed by Efferocytosis Assay kit (cat. no. 601770, Cayman Chemical Company). CD14+ cells were used as effector cells, whereas apoptotic neutrophils were used as target cells. The protocol was re-adapted to use CD14+ monocyte cells rather than differentiated macrophages due to the low cell availability[15]. CD14+ cells were isolated from cryopreserved PBMCs (10 × 10^6 cells) collected following pre-study and 2 weeks post last immunization (week 14) by using non-human primate CD14 MicroBeads (#130-091-097, Miltenyi Biotec) following manufacturer instructions. At the end of the separation, cells were counted and stained with CytoTell Blue (AAT Bioquest) provided by the kit and following manufacturer instructions. One unrelated macaque was used as source of neutrophils as target cells. Neutrophils were isolated of PBMCs by Ficoll Plaque (GE Healthcare), the cellular pellet was added to an equal volume of 20% dextran in water, gently mixed, and incubated for 1 min. Approximately three volumes of PBS were added, mixed again, and incubated in the dark for 50–60 min. At the end of incubation, the clear layer at the top of the tube containing neutrophils was collected. Cells were pelleted and treated with ACK lysing buffer (Quality Biological) for 5 min at 37 °C, washed with R10 and counted. Neutrophils were stained with CFSE provided by the kit following manufacturer instructions. The apoptosis of neutrophils was induced by treatment with Staurosporine Apoptosis inducer provided by the kit. Briefly, isolated cells were resuspended in R10 containing Staurosporine diluted 1:1,000 and incubated at 37 °C for 3 h. At the end of the incubation cells were washed twice with R10 and used for the efferocytosis assay. Subsequently, effector and apoptotic target cells were cultured alone (as controls) or co-cultured at a ratio of one effector CD14+ cell to three target apoptotic neutrophils. Cells were incubated at 37 °C for 12 h. At the end of the co-culture, cells were washed with PBS, fixed with 1% paraformaldehyde in PBS and acquired on a FACSymphony A5 and examined using FACSDiva software (BD Biosciences) by acquiring all stained cells. Data were further analysed using FlowJo v10.6 (TreeStar). The frequency of efferocytotic CD14+ cells was determined as the frequency of double-positive cells for CytoTell Blue and CFSE on the CytoTell Blue-positive monocytes. The efferocytosis assay was done in several experiments, each time paired pre- and post-vaccination was done together. Thus, to combine the experiments for correlation analysis, the post-vaccination efferocytosis (week 14) data were normalized by dividing them with pre-vaccination data and multiplied by 100.

Efferocytosis assay using SAMT-247

Efferocytosis was done as described above with the exception that 100 μM of SAMT-247 were added to the co-culture for 12 h. SAMT-247-induced efferocytosis was measured by subtracting efferocytosis without SAMT-247-treated effector cells from efferocytosis with SAMT-247-treated effector cells.

Intracellular cytokines of human blood NK cells using SAMT-247 and PMA-Ionomycin stimulation with or without zinc chelator

The levels of NKG2A+ NK cells were measured in blood of healthy humans. Human PBMCs were thawed and cultured in R10 in the presence or absence of SAMT-247 and/or PMA-Ionomycin for 12 h. Cells were incubated with or without zinc chelator TPEN (cat. no. P4413-100MG, 5 μM) for 12 h. Subsequently, PBMCs were surface stained with the

following: BUV737 anti-CD3 (SP34-2; cat. no. 741872, 5 μl), Alexa 700 anti-CD20 (2H7; cat. no. 560631, 5 μl), BV786 anti-CD45 (HI30; cat. no. 563716, 5 μl) from BD Biosciences; APC-H7 anti-CD11b (ICRF44; cat. no. 47-0118-42, 5 μl) from eBioscience and PE-Cy7 anti-NKG2A (Z199; cat. no. B10246, 5 μl) from Beckman Coulter for 30 min at room temperature. This was followed by permeabilization with FOXP3-transcription buffer set (cat. no. 00-5523-00) from eBioscience according to the manufacturer's recommendation and subsequent intracellular staining with the following: BV750 anti-TNF-α (MAB11; cat. no. 566359, 5 μl), BUV396 anti-IFN-γ (B27; cat. no. 563563, 5 μl), BV510 anti-GranB (GB11; cat. no. 563388, 5 μl) from BD Biosciences; and FITC anti-Perforin (pf-344; cat. no. 3465-7, 5 μl) from MABTECH for 30 min at room temperature. Flow cytometry acquisitions were performed on a FACSymphony A5 and examined using FACSDiva software (BD Biosciences).

AIM assay

Activation, proliferation and exhaustion markers on Th1 and Th2 cell subsets were measured in blood at week 17 in vaccinated animals using AIM assay[58]. PBMCs were thawed and incubated with CD40 blocking antibody (HB14, cat. no. 130-094-133, 5 μl) from Miltenyi for 15 min, followed by the addition of CD49a (9F10, cat. no. 555501, 2 μl) and CD28 (CD28.2, cat. no. 567117, 2 μl) from BD Bioscience in the presence or absence of gp120 and/or SAMT-247. Cells were incubated at 37 °C for 18 h followed by antibody staining. PBMCs were stained for 30 min at room temperature with the following: LIVE/DEAD Fixable Blue Dead Cell Stain (cat. no. L23105, Thermo Fisher); BV786 anti-CD45 (D058-1283; cat. no. 563861, 5 μl), BUV737 anti-CD3 (SP34-2; cat. no. 741872, 5 μl), BV711 anti-CD4 (L200; cat. no. 740807, 5 μl), BUV496 anti-CD8 (RPA-T8; cat. no. 612942, 5 μl), PE-CF594 anti-PDL1 (MIH1; cat. no. 563742, 5 μl), BB700 anti-CTLA-4 (BNI3; cat. no. 566901, 5 μl), PE-Cy5 anti-OX40 (CD134) (ACT35; cat. no. 551500, 5 μl), BUV563 anti-CD40L (CD154) (24-31; cat. no. 752854, 5 μl), PE-Cy7 anti-CD69 (FN50; cat. no. 557745, 5 μl), PE anti-CD95 (DX2; cat. no. 555674, 5 μl) from BD Bioscience; FITC anti-LAG3 (3DS223H; cat. no. 369326, 5 μl) from Thermofisher; BV750 anti-PD1 (EH12.2H7; cat. no. 329966, 5 μl), Alexa 700 anti-CXCR3 (G025H7; cat. no. 353742, 5 μl), BV605 anti-CCR6 (G034E3; cat. no. 353420, 5 μl) from BioLegend. Staining was followed by permeabilization with a FOXP3-transcription buffer set (cat. no. 00-5523-00) from eBioscience according to the manufacturer's recommendation and subsequently stained intracellularly with BV510 anti-Ki67 (B56; cat. no. 563462, 5 μl) from BD Biosciences for 30 min at room temperature. Samples were acquired on a BD FACSymphony A5 cytometer and analysed with FlowJo software 10.6. Th1 cells were gated as singlets, live cells, CD45+ cells, CD3+, CD4+, CD8−, CD95+, CXCR3+, CCR6−; Th2 cells were gated as singlets, live cells, CD45+ cells, CD3+, CD4+, CD8−, CD95+, CXCR3−, CCR6−. Activation, proliferation and exhaustion markers were gated on parent population.

Intracellular cytokines of macaque blood NK cells and T cells using SAMT-247 and gp120 stimulation with or without zinc chelator

The levels of NKG2A+ NK cells and T cells were measured in blood of vaccinated macaques. Macaque PBMCs were thawed and cultured in R10 in the presence or absence of SAMT-247 and/or gp120 pooled peptides for 12 h. Cells were incubated with or without zinc chelator TPEN (cat. no. P4413-100MG, 5 μM) for 12 h. Subsequently, cells were stained for live cells with Live/Dead Blue dye (cat. no. L34962, 0.5 μl) from Thermo Fisher; followed by surface staining with the following: PE anti-CD45 (D058-1283; cat. no. 552833, 5 μl), BB700 anti-CD3 (RPA-T8; cat. no. 566452, 5 μl), Alexa 700 anti-CD3 (SP34-2; cat. no. 557917, 5 μl), BV711 anti-CD4 (L200; cat. no. 563913, 5 μl), BV786 anti-CCR5 (3A9; cat. no. 565001, 5 μl), BUV737 anti-CD20 (2H7; cat. no. 612848, 5 μl), BUV496 anti-CD16 (3G8; cat. no. 612944, 5 μl), BUV661 anti-HLA-DR (G46-6; cat. no. 612980, 5 μl), BUV805 anti-CD14 (M5E2; cat. no. 565779, 5 μl) from BD Biosciences; APC-H7 anti-CD11b (ICRF44; cat. no. 47-0118-42, 5 μl),

PE-Cy5 anti-CD95 (DX2; cat. no. 15-0959-42, 5 µl) from eBioscience; PE-Cy7 anti-NKG2A (Z199; cat. no. B10246, 5 µl) from Beckman Coulter; APC anti-$\alpha_4\beta_7$ (A4B7R1; cat. no. 051514AB, 5 µl) by the NIH Nonhuman Primate Reagent Resource (R24 OD010976, and NIAID contract HHSN272201300031C), and BV605 anti-CCR6 (G034E3; cat. no. 353420, 5 µl), BV650 anti-CXCR3 (G025H7; cat. no. 353730, 5 µl) from BioLegend for 30 min at room temperature. This was followed by permeabilization with FOX3-transcription buffer set (cat. no. 00-5523-00) from eBioscience according to the manufacturer's recommendation and subsequent intracellular staining with the following: BV750 anti-TNF-α (MAB11; cat. no. 566359, 5 µl), BUV396 anti-IFN-γ (B27; cat. no. 563563, 5 µl), BV510 anti-GranB (GB11; cat. no. 563388, 5 µl), BV421 anti-IL-10 (JES3-9D7; cat. no. 564053, 5 µl), PE-CF594 anti-Ki67 (B56; cat. no. 567120, 5 µl) from BD Biosciences; and FITC anti-Perforin (pf-344; cat. no. 3465-7, 5 µl) from MABTECH for 30 min at room temperature. Flow cytometry acquisitions were performed on a FACSymphony A5 and examined using FACSDiva software (BD Biosciences).

Frequencies and cytokine levels of macaque rectal mucosal NK cells and T cells following SAMT-247 and PMA-Ionomycin stimulation

NK/ILC and T-cell frequencies and cytokine levels were measured in macaque rectal mucosa. Freshly collected rectal biopsies were processed to single cells and cultured in R10 in the presence/or absence of SAMT-247 and/or PMA-Ionomycin for 12 h. Subsequently, cells were stained for live cells with Live/Dead Blue dye (cat. no. L34962, 0.5 µl) from Thermo Fisher; followed by surface staining with the following: BUV737 anti-CD3 (SP34-2; cat. no. 741872, 5 µl), BV711 anti-CD4 (L200; cat. no. 563913, 5 µl), BV650 anti-NKp44 (P44-8; cat. no. 744302, 5 µl), Alexa 700 anti-CD20 (2H7; cat. no. 560631, 5 µl), BV786 anti-CD45 (D058-1283; cat. no. 563861, 5 µl) from BD Biosciences; APC-H7 anti-CD11b (ICRF44; cat. no. 47-0118-42, 5 µl), PE-Cy5 anti-CD95 (ICRF44; cat. no. 15-0959-42, 5 µl) from eBioscience; BV570 anti-CD8 (RPA-T8; cat. no. 301038, 5 µl), BV605 anti-CCR6 (G034E3; cat. no. 353420, 5 µl), APC anti-CXCR3 (G025H7; cat. no. 353708, 5 µl), from BioLegend and PE-Cy7 anti-NKG2A (Z199; cat. no. B10246, 5 µl) from Beckman Coulter for 30 min at room temperature. This was followed by permeabilization with a FOXP3-transcription buffer set (cat. no. 00-5523-00) from eBioscience according to the manufacturer's recommendation and subsequent intracellular staining with the following: BV750 anti-TNF-α (MAB11; cat. no. 566359, 5 µl), BUV395 anti-IFN-γ (B27; cat. no. 563563, 5 µl), BV510 anti-GranB (GB11; cat. no. 563388, 5 µl), BV421 anti-IL-10 (JES3-9D7; cat. no. 564053, 5 µl) from BD Biosciences; PE-Cy5.5 anti-IL-17 (BL168; cat. no. 512314, 5 µl) from BioLegend; and FITC anti-Perforin (pf-344; cat. no. 3465-7, 5 µl) from MABTECH for 30 min at room temperature. Flow cytometry acquisitions were performed on a FACSymphony A5 and examined using FACSDiva software (BD Biosciences).

Zinc intensity

NKG2A⁺ NK cells were isolated from cryopreserved healthy human PBMCs. NK cells were labelled with APC anti-NKG2A (Z199, cat. no. A60797) from Beckman Coulter and Aqua Live/Dead viability dye was used to exclude dead cells. After staining, cells were washed, passed through a 40 µm cell strainer, and sorted on an Astrios EQ flow cytometer. NKG2A⁺ of live cells were sorted with purity of 99%. Subsequently, NK cells were cultured in the presence or absence of SAMT-247 and/or PMA-Ionomycin stimulation for 7 h. Cells were plated on ibidi chamber slides. Cells were washed and treated with zinc chelator or remained untreated for 30 min according to the manufacturer recommendation using a cell-based zinc assay kit (cat. no. ab241014, Abcam). Subsequently, cells were washed and stained with zinc probe-green (cat. no. ab241014, Abcam) and DAPI (Molecular Probes) was used to visualize nuclei. Signals were visualized with a confocal laser-scanning microscope (Leica SP8, Leica Microsystems). Image processing was performed using the Imaris 9.2.1 software (Oxford Instruments).

Statistical analysis

Statistical analysis was performed without testing normal distribution and equal variances of the data, and therefore non-parametric tests were used. The two-tailed Wilcoxon signed-rank test or two-tailed Mann–Whitney test was used to compare continuous factors between two paired or unpaired groups, respectively. Comparisons of differences between groups in the number of challenges before viral acquisition were assessed using the log-rank (Mantel–Cox) test of the discrete-time proportional hazards model. The average per-risk challenge of viral acquisition was estimated as the total number of observed infections divided by the number of administered challenges. Correlation analyses were performed using the non-parametric Spearman-rank correlation method with exact permutation and approximate two-tailed P values calculated for the number of pairs ≤17 and >17, respectively. Since this research was conducted as exploratory, all P values are reported as nominal values without adjusting for multiple comparisons. No animals or data points were excluded from the analyses.

Reporting summary

Further information on research design is available in the Nature Portfolio Reporting Summary linked to this article.

Data availability

All data in the manuscript and supplemental material are provided in the accompanying 'Source Data' files. Source data are provided with this paper.

Code availability

N/A.

References

1. UNAIDS. *FACT SHEET – WORLD AIDS DAY 2021* Vol. 2022 (UNAIDS, 2021).
2. Birdthistle, I. et al. Recent levels and trends in HIV incidence rates among adolescent girls and young women in ten high-prevalence African countries: a systematic review and meta-analysis. *Lancet Glob. Health* **7**, e1521–e1540 (2019).
3. Flynn, N. M. et al. Placebo-controlled phase 3 trial of a recombinant glycoprotein 120 vaccine to prevent HIV-1 infection. *J. Infect. Dis.* **191**, 654–665 (2005).
4. Pitisuttithum, P. et al. Randomized, double-blind, placebo-controlled efficacy trial of a bivalent recombinant glycoprotein 120 HIV-1 vaccine among injection drug users in Bangkok, Thailand. *J. Infect. Dis.* **194**, 1661–1671 (2006).
5. Buchbinder, S. P. et al. Efficacy assessment of a cell-mediated immunity HIV-1 vaccine (the Step Study): a double-blind, randomised, placebo-controlled, test-of-concept trial. *Lancet* **372**, 1881–1893 (2008).
6. Gray, G. E. et al. Safety and efficacy of the HVTN 503/Phambili study of a clade-B-based HIV-1 vaccine in South Africa: a double-blind, randomised, placebo-controlled test-of-concept phase 2b study. *Lancet Infect. Dis.* **11**, 507–515 (2011).
7. Gray, G. E. et al. Recombinant adenovirus type 5 HIV gag/pol/nef vaccine in South Africa: unblinded, long-term follow-up of the phase 2b HVTN 503/Phambili study. *Lancet Infect. Dis.* **14**, 388–396 (2014).
8. Rerks-Ngarm, S. et al. Vaccination with ALVAC and AIDSVAX to prevent HIV-1 infection in Thailand. *N. Engl. J. Med.* **361**, 2209–2220 (2009).
9. Hammer, S. M. et al. Efficacy trial of a DNA/rAd5 HIV-1 preventive vaccine. *N. Engl. J. Med.* **369**, 2083–2092 (2013).
10. Gray, G. E. et al. Vaccine efficacy of ALVAC-HIV and bivalent subtype C gp120-MF59 in adults. *N. Engl. J. Med.* **384**, 1089–1100 (2021).

11. A study to assess the efficacy of a heterologous prime/boost vaccine regimen of Ad26.Mos4.HIV and aluminum phosphate-adjuvanted clade C gp140 in preventing human immunodeficiency virus (HIV)-1 infection in women in Sub-Saharan Africa. *NIH* https://ClinicalTrials.gov/show/NCT03060629 (2022).

12. A study of heterologous vaccine regimen of adenovirus serotype 26 Mosaic4 human immunodeficiency virus (Ad26.Mos4.HIV), adjuvanted clade C gp140 and Mosaic gp140 to prevent HIV-1 infection among cis-gender men and transgender individuals who have sex with cis-gender men and/or transgender individuals. *NIH* https://ClinicalTrials.gov/show/NCT03964415 (2023).

13. Vaccari, M. et al. Adjuvant-dependent innate and adaptive immune signatures of risk of SIVmac251 acquisition. *Nat. Med.* **22**, 762–770 (2016).

14. Vaccari, M. et al. HIV vaccine candidate activation of hypoxia and the inflammasome in CD14+ monocytes is associated with a decreased risk of SIVmac251 acquisition. *Nat. Med.* **24**, 847–856 (2018).

15. Bissa, M. et al. HIV vaccine candidate efficacy in female macaques mediated by cAMP-dependent efferocytosis and V2-specific ADCC. *Nat. Commun.* **14**, 575 (2023).

16. Silva de Castro, I. et al. Anti-V2 antibodies virus vulnerability revealed by envelope V1 deletion in HIV vaccine candidates. *iScience* **24**, 102047 (2021).

17. Haynes, B. F. et al. Immune-correlates analysis of an HIV-1 vaccine efficacy trial. *N. Engl. J. Med.* **366**, 1275–1286 (2012).

18. Goes, L. R. et al. The V2 loop of HIV gp120 delivers costimulatory signals to CD4+ T cells through Integrin alpha4beta7 and promotes cellular activation and infection. *Proc. Natl Acad. Sci. USA* **117**, 32566–32573 (2020).

19. Gschwandtner, M., Derler, R. & Midwood, K. S. More than just attractive: how CCL2 influences myeloid cell behavior beyond chemotaxis. *Front. Immunol.* **10**, 2759 (2019).

20. Tomalka, J. A. et al. The transcription factor CREB1 is a mechanistic driver of immunogenicity and reduced HIV-1 acquisition following ALVAC vaccination. *Nat. Immunol.* **22**, 1294–1305 (2021).

21. Negreiros-Lima, G. L. et al. Cyclic AMP regulates key features of macrophages via PKA: recruitment, reprogramming and efferocytosis. *Cells* **9**, 128 (2020).

22. Doran, A. C., Yurdagul, A. Jr. & Tabas, I. Efferocytosis in health and disease. *Nat. Rev. Immunol.* **20**, 254–267 (2020).

23. Rahman, M. A. et al. Differential effect of mucosal NKp44+ innate lymphoid cells and deltagamma cells on simian immunodeficiency virus infection outcome in rhesus macaques. *J. Immunol.* **203**, 2459–2471 (2019).

24. Turpin, J. A., Schito, M. L., Jenkins, L. M., Inman, J. K. & Appella, E. Topical microbicides: a promising approach for controlling the AIDS pandemic via retroviral zinc finger inhibitors. *Adv. Pharm.* **56**, 229–256 (2008).

25. Jenkins, L. M. et al. Studies on the mechanism of inactivation of the HIV-1 nucleocapsid protein NCp7 with 2-mercaptobenzamide thioesters. *J. Med. Chem.* **48**, 2847–2858 (2005).

26. Turpin, J. A. et al. Inhibitors of human immunodeficiency virus type 1 zinc fingers prevent normal processing of gag precursors and result in the release of noninfectious virus particles. *J. Virol.* **70**, 6180–6189 (1996).

27. Miller Jenkins, L. M. et al. Small-molecule inactivation of HIV-1 NCp7 by repetitive intracellular acyl transfer. *Nat. Chem. Biol.* **6**, 887–889 (2010).

28. Wallace, G. S. et al. Human immunodeficiency virus type 1 nucleocapsid inhibitors impede trans infection in cellular and explant models and protect nonhuman primates from infection. *J. Virol.* **83**, 9175–9182 (2009).

29. Schito, M. L. et al. In vivo antiviral activity of novel human immunodeficiency virus type 1 nucleocapsid p7 zinc finger inhibitors in a transgenic murine model. *AIDS Res. Hum. Retroviruses* **19**, 91–101 (2003).

30. Cheng-Mayer, C. et al. Delay of simian human immunodeficiency virus infection and control of viral replication in vaccinated macaques challenged in the presence of a topical microbicide. *AIDS* **25**, 1833–1841 (2011).

31. Helmold Hait, S. et al. An SAMT-247 microbicide provides potent protection against intravaginal simian immunodeficiency virus infection of rhesus macaques, whereas an added vaccine component elicits mixed outcomes. *J. Immunol.* **204**, 3315–3328 (2020).

32. Henson, P. M. Cell removal: efferocytosis. *Annu. Rev. Cell Dev. Biol.* **33**, 127–144 (2017).

33. Cicala, C. et al. The integrin alpha4beta7 forms a complex with cell-surface CD4 and defines a T-cell subset that is highly susceptible to infection by HIV-1. *Proc. Natl Acad. Sci. USA* **106**, 20877–20882 (2009).

34. Kader, M., Bixler, S., Roederer, M., Veazey, R. & Mattapallil, J. J. CD4 T cell subsets in the mucosa are CD28+Ki-67−HLA−DR−CD69+ but show differential infection based on alpha4beta7 receptor expression during acute SIV infection. *J. Med. Primatol.* **38**, 24–31 (2009).

35. Redmond, W. L., Ruby, C. E. & Weinberg, A. D. The role of OX40-mediated co-stimulation in T-cell activation and survival. *Crit. Rev. Immunol.* **29**, 187–201 (2009).

36. Blair, P. J. et al. CD40 ligand (CD154) triggers a short-term CD4+ T cell activation response that results in secretion of immunomodulatory cytokines and apoptosis. *J. Exp. Med.* **191**, 651–660 (2000).

37. Cibrian, D. & Sanchez-Madrid, F. CD69: from activation marker to metabolic gatekeeper. *Eur. J. Immunol.* **47**, 946–953 (2017).

38. Soares, A. et al. Novel application of Ki67 to quantify antigen-specific in vitro lymphoproliferation. *J. Immunol. Methods* **362**, 43–50 (2010).

39. Parry, R. V. et al. CTLA-4 and PD-1 receptors inhibit T-cell activation by distinct mechanisms. *Mol. Cell. Biol.* **25**, 9543–9553 (2005).

40. Blank, C. & Mackensen, A. Contribution of the PD-L1/PD-1 pathway to T-cell exhaustion: an update on implications for chronic infections and tumor evasion. *Cancer Immunol. Immunother.* **56**, 739–745 (2007).

41. Tian, X. et al. The upregulation of LAG-3 on T cells defines a subpopulation with functional exhaustion and correlates with disease progression in HIV-infected subjects. *J. Immunol.* **194**, 3873–3882 (2015).

42. Read, S. A., Obeid, S., Ahlenstiel, C. & Ahlenstiel, G. The role of zinc in antiviral immunity. *Adv. Nutr.* **10**, 696–710 (2019).

43. Prasad, A. S., Miale, A. Jr., Farid, Z., Sandstead, H. H. & Schulert, A. R. Zinc metabolism in patients with the syndrome of iron deficiency anemia, hepatosplenomegaly, dwarfism, and hypognadism. *J. Lab. Clin. Med.* **61**, 537–549 (1963).

44. Tone, K., Suzuki, T. & Todoroki, T. Influence of zinc deficiency on phagocytosis in mice. *Kitasato Arch. Exp. Med* **64**, 263–269 (1991).

45. Wirth, J. J., Fraker, P. J. & Kierszenbaum, F. Zinc requirement for macrophage function: effect of zinc deficiency on uptake and killing of a protozoan parasite. *Immunology* **68**, 114–119 (1989).

46. Hamon, R. et al. Zinc and zinc transporters in macrophages and their roles in efferocytosis in COPD. *PLoS ONE* **9**, e110056 (2014).

47. Haase, H. et al. Zinc signals are essential for lipopolysaccharide-induced signal transduction in monocytes. *J. Immunol.* **181**, 6491–6502 (2008).

48. Jenkins, J. L. & Urban, L. Phenotypic screening: fishing for neuroactive compounds. *Nat. Chem. Biol.* **6**, 172–173 (2010).

49. Miller Jenkins, L. M. et al. Inhibition of HIV maturation via selective unfolding and cross-linking of Gag polyprotein by a mercaptobenzamide acetylator. *J. Am. Chem. Soc.* **141**, 8327–8338 (2019).

50. Lambert, S. A. et al. The human transcription factors. *Cell* **172**, 650–665 (2018).

51. Andreini, C. & Bertini, I. A bioinformatics view of zinc enzymes. *J. Inorg. Biochem.* **111**, 150–156 (2012).

52. Gammoh, N. Z. & Rink, L. Zinc in infection and inflammation. *Nutrients* **9**, 624 (2017).

53. Wessels, I., Maywald, M. & Rink, L. Zinc as a gatekeeper of immune function. *Nutrients* **9**, 1286 (2017).

54. Sheikh, A. et al. Zinc influences innate immune responses in children with enterotoxigenic *Escherichia coli*-induced diarrhea. *J. Nutr.* **140**, 1049–1056 (2010).

55. Kjellerup, L., Winther, A. L., Wilson, D. & Fuglsang, A. T. Cyclic AMP pathway activation and extracellular zinc induce rapid intracellular zinc mobilization in *Candida albicans*. *Front. Microbiol.* **9**, 502 (2018).

56. Kido, T., Suka, M. & Yanagisawa, H. Effectiveness of interleukin-4 administration or zinc supplementation in improving zinc deficiency-associated thymic atrophy and fatty degeneration and in normalizing T cell maturation process. *Immunology* **165**, 445–459 (2022).

57. Orlandi, C., Flinko, R. & Lewis, G. K. A new cell line for high throughput HIV-specific antibody-dependent cellular cytotoxicity (ADCC) and cell-to-cell virus transmission studies. *J. Immunol. Methods* **433**, 51–58 (2016).

58. Reiss, S. et al. Comparative analysis of activation induced marker (AIM) assays for sensitive identification of antigen-specific CD4 T cells. *PLoS ONE* **12**, e0186998 (2017).

Author contributions

G.F. and M.R.-G. conceived the study. M.A.R. and G.F. wrote the paper, with contributions from all authors; M.A.R. coordinated the macaque studies, performed ADCC assay, zinc inhibition assay, mucosal innate response analysis, phenotyping and intracellular cytokine assays, AIM assay, analysed the data, and prepared the figures; M.B. performed efferocytosis assay, cellular assays and coordinated the macaque studies and processed samples; I.S.d.C. coordinated the macaque studies and performed T-cell assays and processed samples; S.H.H. coordinated the macaque studies and processed samples; J.D.S. performed T-cell assays; F.B. performed the fluorescence microscopy assays and analysed the data; R.H., S.S., A.G., M.N.D., R.M. and T.H. processed samples and performed experiments; L.M.M.-J., E.A. and D.H.A. provided SAMT-247 microbicide and HEC gel; T.C. contributed to the study design; M.M.B. oversaw the in vitro drug and gel stability studies and analysed the data. D.J.V. and H.C.-W. performed statistical analysis of the data.

Competing interests

The authors declare no competing financial interests. The US government filed Patent No. 63/228,707: HIV vaccination and SAMT-247 microbicide to prevent HIV infection.

Additional information

Extended data is available for this paper at https://doi.org/10.1038/s41564-023-01353-7.

Supplementary information The online version contains supplementary material available at https://doi.org/10.1038/s41564-023-01353-7.

Correspondence and requests for materials should be addressed to Genoveffa Franchini.

Peer review information *Nature Microbiology* thanks Mirko Paiardini, Rama Amara and Steven de Rosa for their contribution to the peer review of this work.

Reprints and permissions information is available at www.nature.com/reprints.

Publisher's note Springer Nature remains neutral with regard to jurisdictional claims in published maps and institutional affiliations.

Extended Data Fig. 1 | Assessment of infection rate in different animal groups. a) No differences in delayed acquisition in the concurrent control group were observed compared to the historical controls ($P = 0.74$). Significant protection or trend of protection in **b, c**) the vaccine group ($P = 0.006$ and $P = 0.18$, respectively) and **d, e**) vaccine+SAMT-247 group ($P = 0.0002$ and $P < 0.0001$, respectively) compared with concurrent or historical controls. **f, g**) No differences in delayed acquisition in the SAMT-247 group were observed compared to concurrent ($P = 0.59$) or historical controls ($P = 0.24$). Data shown in (**a-g**) were analyzed with log-rank (Mantel–Cox) test.
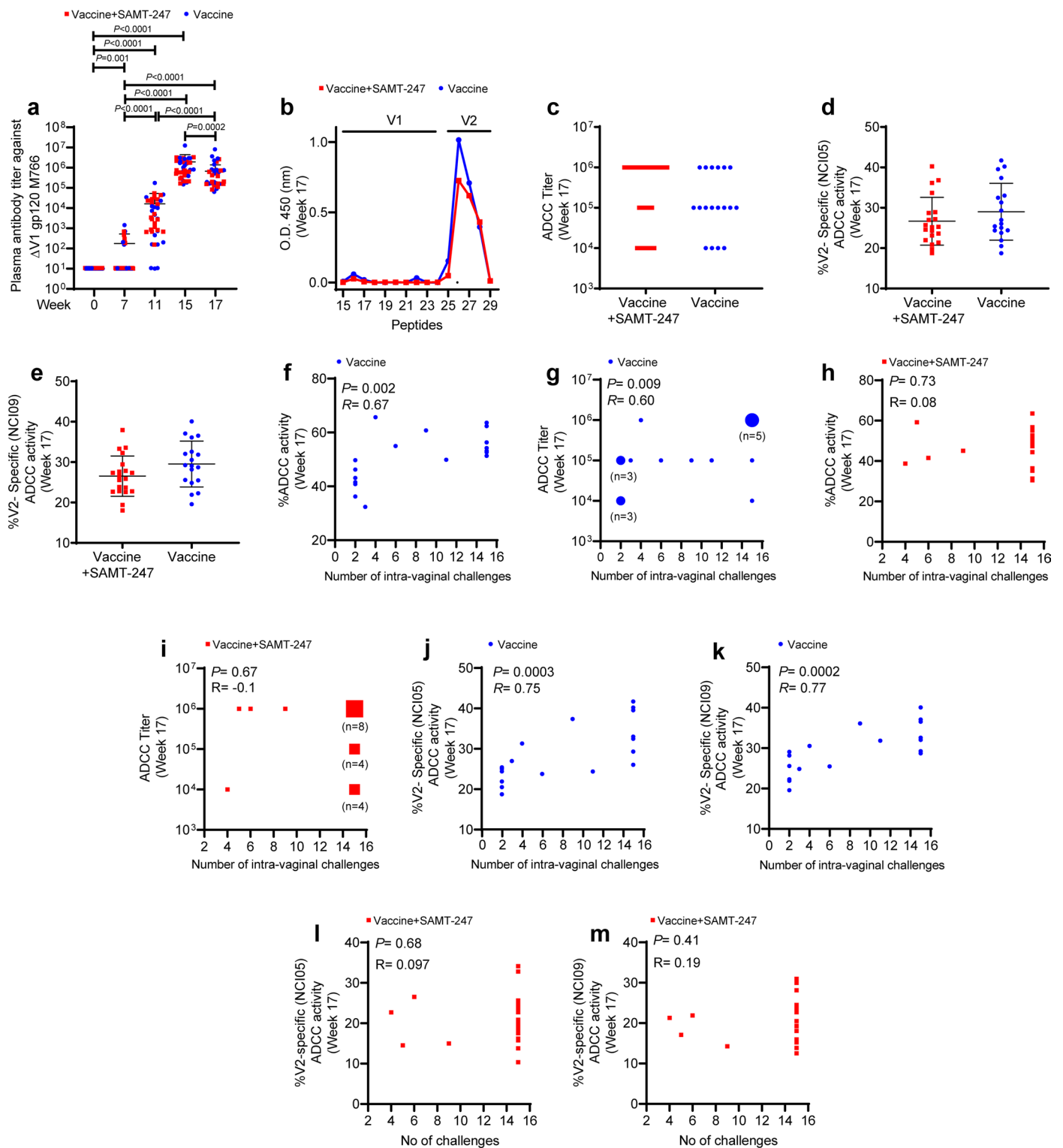
Extended Data Fig. 2 | Quantification of humoral responses in plasma of vaccinated rhesus macaques. a) Plasma antibody titers against ΔV1 gp120 over the course of immunization in the vaccine+SAMT-247 group (n = 20) and vaccine group (n = 18). **b)** Plasma antibody responses against different peptides encompassing V1 (peptides 15–24) and V2 (peptides 25–29) loop regions of gp120 in the vaccine+SAMT-247 group (n = 20) and vaccine group (n = 18). **(c-e)** Comparison of **c)** ADCC titer (*P* = 0.44), **d)** V2-specific (NCI05-specific) ADCC activity (*P* = 0.33) and **e)** V2-specific (NCI09-specific) ADCC activity (*P* = 0.13) at week 17 in the vaccine+SAMT-247 group (n = 20) and vaccine group

(n = 18). **(f-g)** Correlation of **f)** ADCC activity and **g)** ADCC titer in the vaccine group (n = 18). **(h-i)** Correlation of **h)** ADCC activity and **i)** ADCC titer in the vaccine+SAMT-247 group (n = 20), **(j-m)** V2-specific (NCI05 and NCI09-specific) ADCC activity with number of intra-vaginal challenges in the vaccine group (n = 18) and vaccine+SAMT-247 group (n = 20). Data shown in (**a, c-e**) were analyzed with the two-tailed Wilcoxon signed-rank test or two-tailed Mann-Whitney test. Data shown in (**f-m**) were analyzed with the two-tailed Spearman correlation test. Horizontal and vertical bars denote mean and SD.
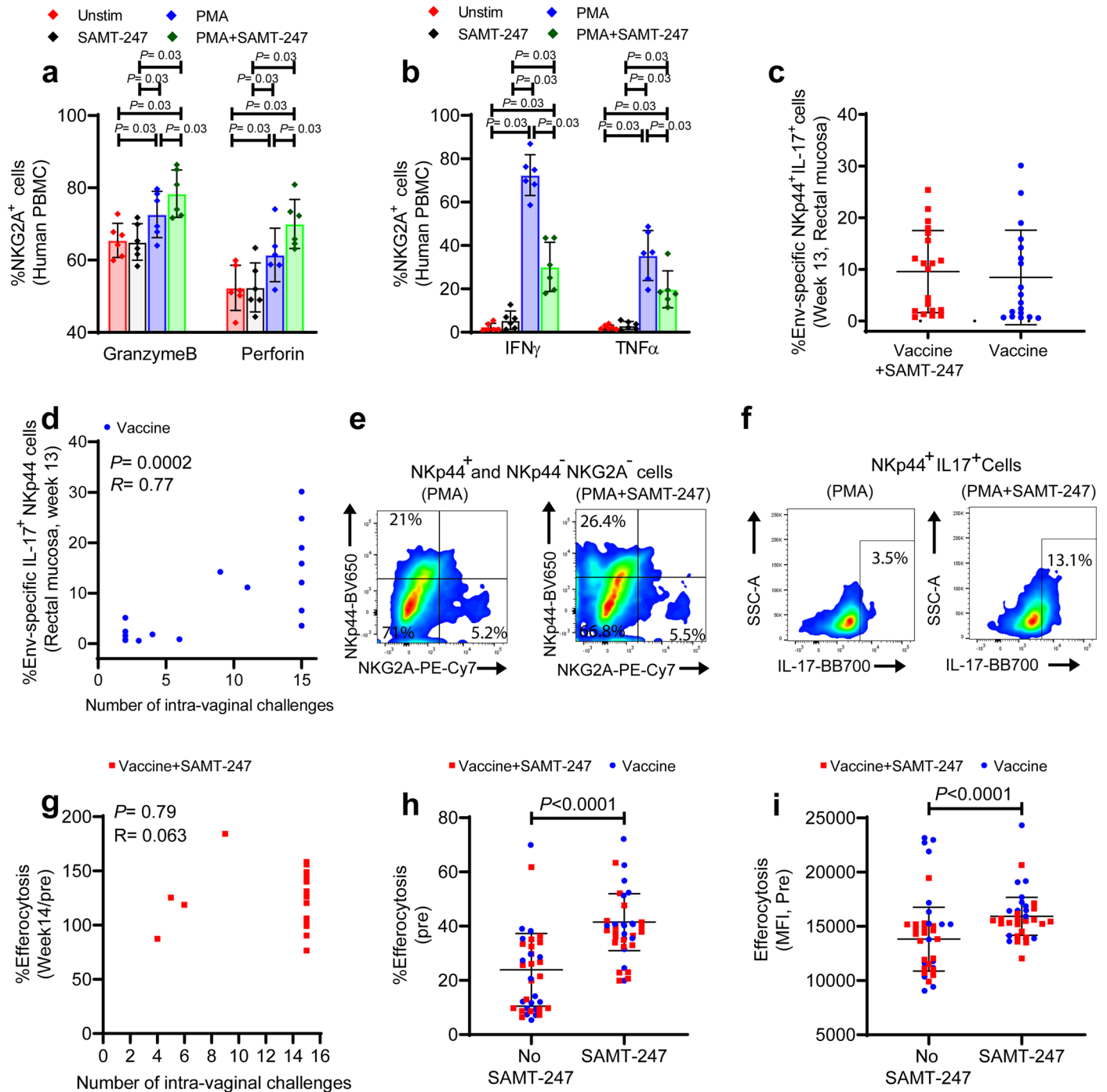
Extended Data Fig. 3 | Evaluation of NK/ILCs response and efferocytosis in humans and in rhesus macaques. a, b) Intracellular Granzyme B, perforin, IFN-γ, and TNF-α in healthy human (n = 6) blood NKG2A⁺ cells in the presence or absence of different stimuli. **c)** Comparison of Env-specific rectal NKp44⁺IL-17⁺ cells between vaccine+SAMT-247 (n = 20) and vaccine group (n = 18) 1 week post last vaccination (P = 0.43). **d)** Correlation of rectal mucosal Env-specific NKp44⁺IL-17⁺ cells with number of intra-vaginal challenges in the vaccine group (n = 18). **e)** Gating of NKG2A⁺NK cells, NKp44⁺ILCs, and NKG2A⁻NKp44⁻ILCs in rectal mucosal samples in the presence of PMA or PMA + SAMT-247 at 12 hours post stimulation. Gating was done on singlets, live, CD45⁺, CD3⁻,

CD20⁻, CD11b⁻ cells. **f)** Gating of NKp44⁺IL-17⁺ ILCs in the rectal mucosal sample in the presence of PMA or PMA + SAMT-247 at 12 hours post stimulation. **g)** Correlation of efferocytosis percentage with number of intra-vaginal challenges in the vaccine+SAMT-247 group (n = 20). **(h-i)** Comparison of **h)** percentage of efferocytosis (P < 0.0001) and **i)** efferocytosis MFI (P < 0.0001) using pre CD14⁺ monocytes in all vaccinated animals (n = 38). Data shown in (**a, b, h, i**) were analyzed with the two-tailed Wilcoxon signed-rank test or two-tailed Mann-Whitney test. Data shown in (**d, g**) were analyzed with the two-tailed Spearman correlation test.
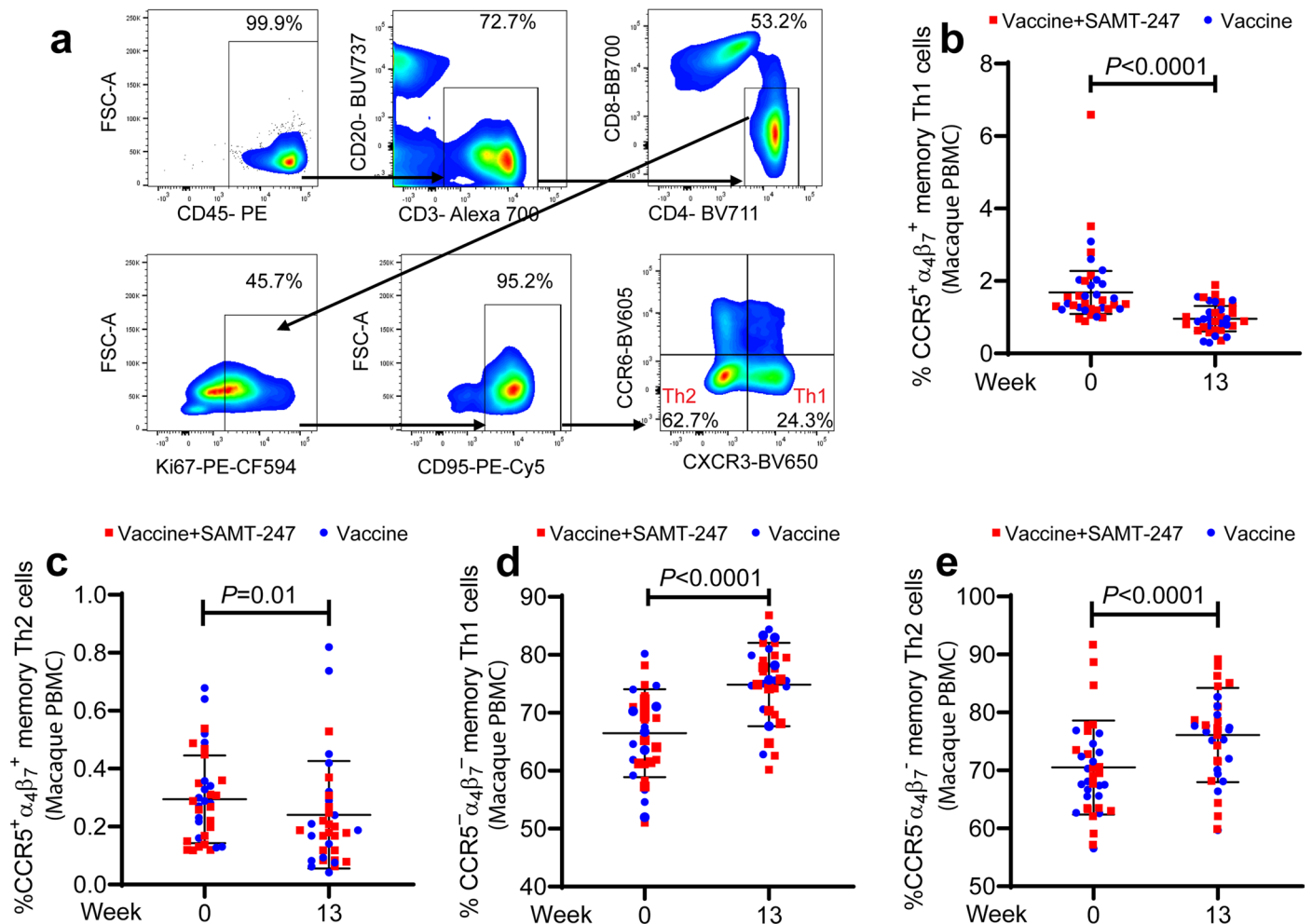
Extended Data Fig. 4 | Determination of *ex vivo* macaque T-cell responses.
a) Gating strategy of Th1 and Th2 cells, **b,c**) Comparison of CCR5$^+\alpha_4\beta_7^+$ ($P < 0.0001$ and $P = 0.01$, respectively) and **d,e**) CCR5$^-\alpha_4\beta_7^-$ memory ($P < 0.0001$ and $P < 0.0001$, respectively) Th1 and Th2 cells pre vaccination and at 1 week post last vaccination (week 13) in blood (n = 38). Data shown in (**b-e**) were analyzed with the two-tailed Wilcoxon signed-rank test. Horizontal and vertical bars denote mean and SD.
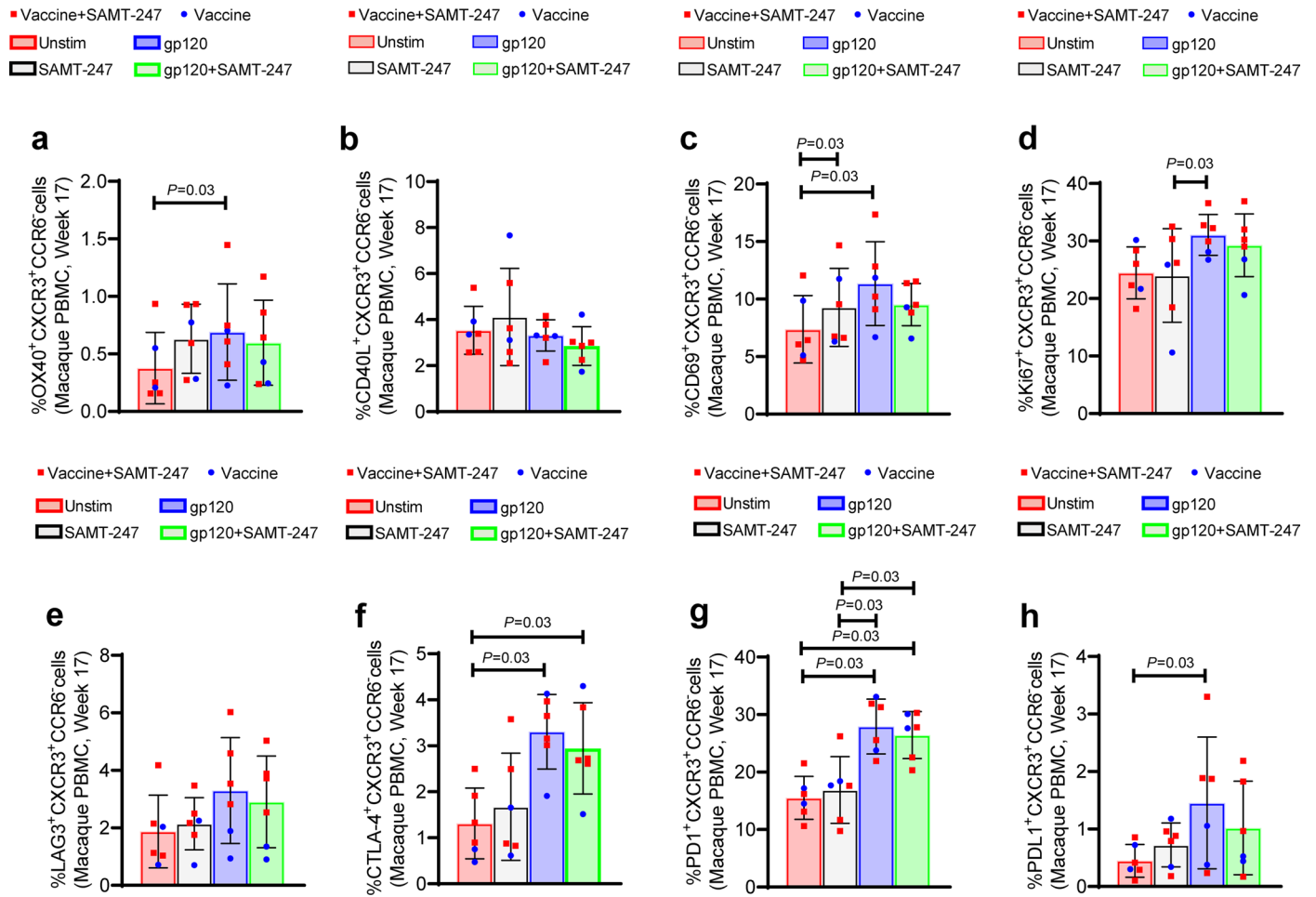
Extended Data Fig. 5 | Quantification of activation, proliferation and exhaustion marker on Th1 cells upon stimulation. Expression of **a)** OX40, **b)** CD40L, **c)** CD69, **d)** Ki67, **e)** LAG3, **f)** CTLA-4, **g)** PD-1 and **h)** PDL-1 in Th1 cells upon stimulation in the vaccine+SAMT-247 group (n = 4) and vaccine group (n = 2). Data shown in (**a-h**) were analyzed with the two-tailed Wilcoxon signed-rank test. Horizontal and vertical bars denote mean and SD.
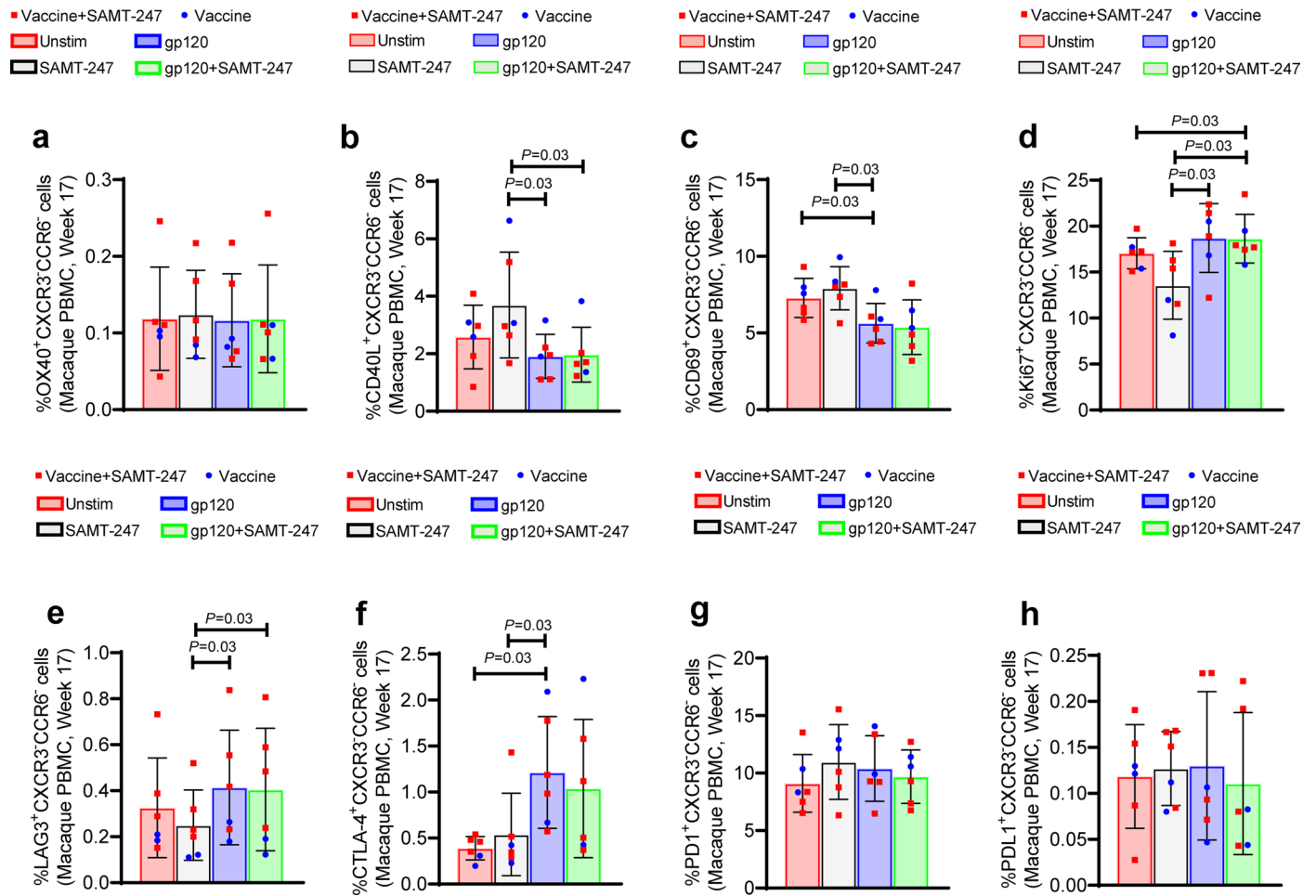
Extended Data Fig. 6 | Evaluation of activation, proliferation and exhaustion marker on Th2 cells upon stimulation. Expression of **a**) OX40, **b**) CD40L, **c**) CD69, **d**) Ki67, **e**) LAG3, **f**) CTLA-4, **g**) PD-1 and **h**) PDL-1 in Th2 cells upon stimulation in the vaccine+SAMT-247 group (n = 4) and vaccine group (n = 2). Data shown in (**a-h**) were analyzed with the two-tailed Wilcoxon signed-rank test. Horizontal and vertical bars denote mean and SD.
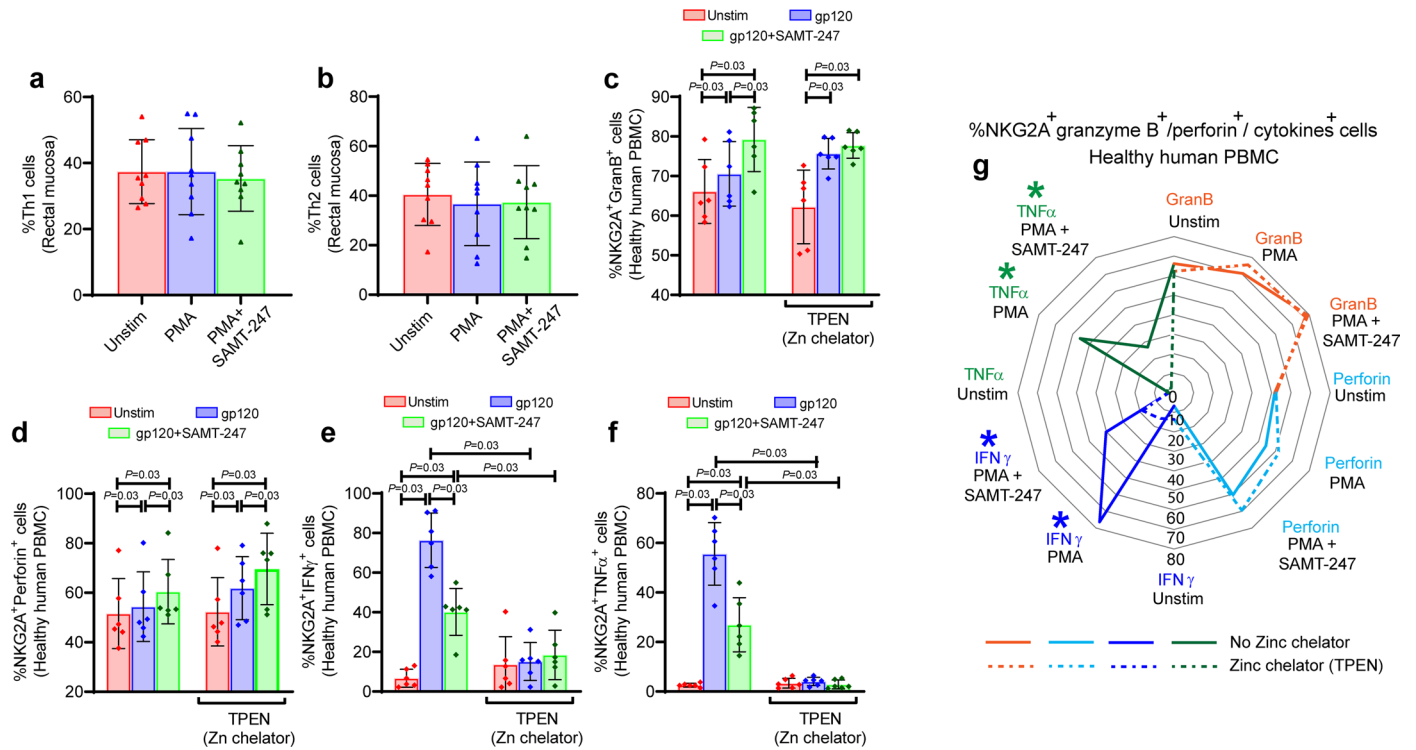
Extended Data Fig. 7 | Quantification of macaque mucosal T-cell responses and human NK cell responses. a, b) Frequency of Th1 cells and Th2 cells in the rectal mucosa of macaques (n = 9). **c-g)** Comparison of expressions of granzyme B, perforin, IFN-γ and TNF-α by NKG2A⁺ cells from healthy humans (n = 6) in the absence or presence of zinc chelator and stimuli (n = 6). Data shown in (**a-g**) were analyzed with the two-tailed Wilcoxon signed-rank test. Horizontal and vertical bars denote mean and SD. The radar plot represents the mean percentage value of cytokine responses. Solid lines represent the absence of zinc chelator and dashed lines represent the presence of zinc chelator.
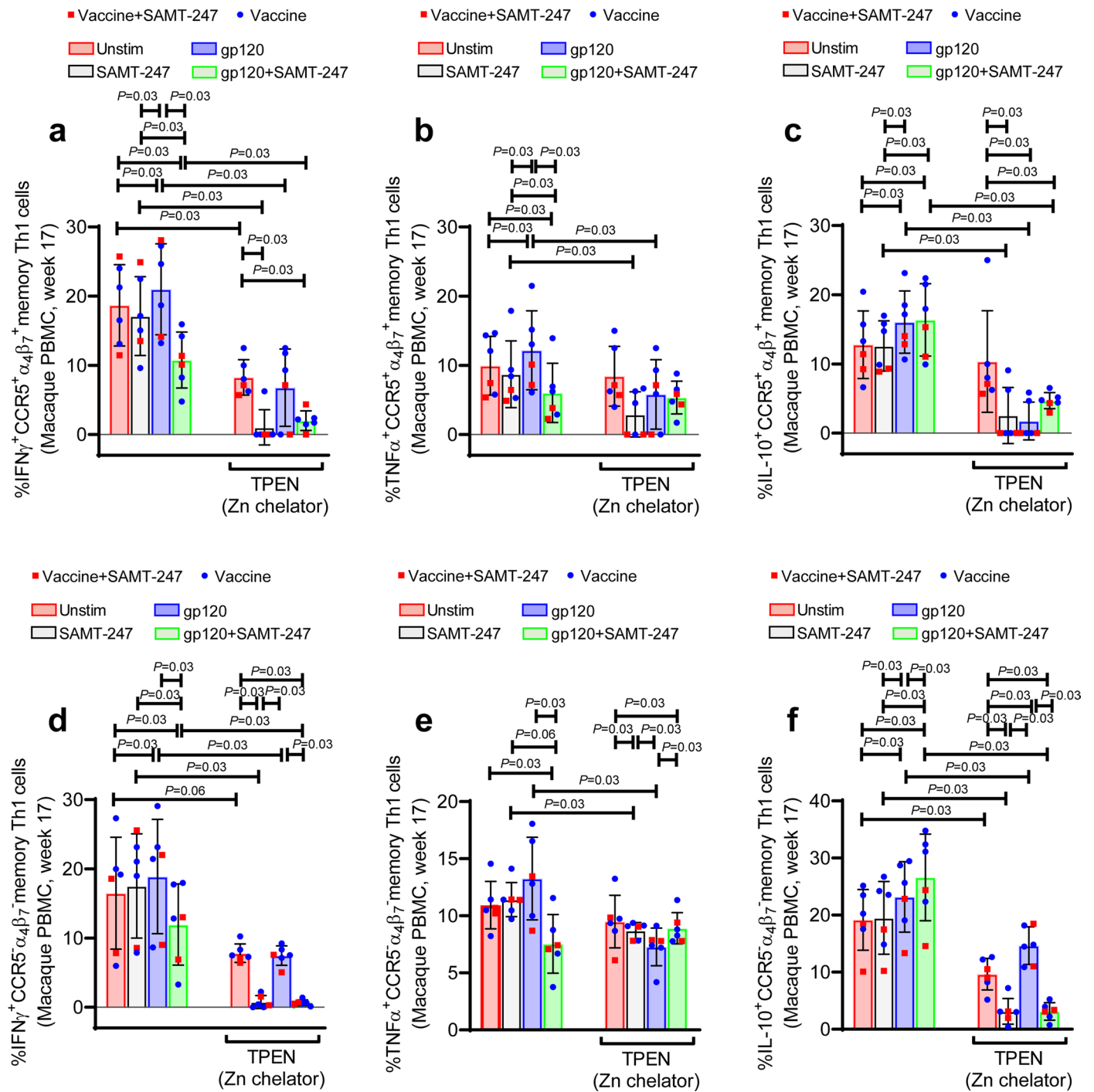
Extended Data Fig. 8 | Comparison of cytokine responses by CCR5⁺α₄β₇⁺ and CCR5⁻α₄β₇⁻ memory Th1 cells in the presence of stimulation. a-f) Comparison of intracellular expressions of IFN-γ, TNF-α, and IL-10 by CCR5⁺α₄β₇⁺ and CCR5⁻α₄β₇⁻ Th1 memory cells in the absence or presence of zinc chelator and stimuli in the vaccine+SAMT-247 group (n = 4) and vaccine group (n = 2). Data shown in (**a-f**) were analyzed with the two-tailed Wilcoxon signed-rank test. Horizontal and vertical bars denote mean and SD.
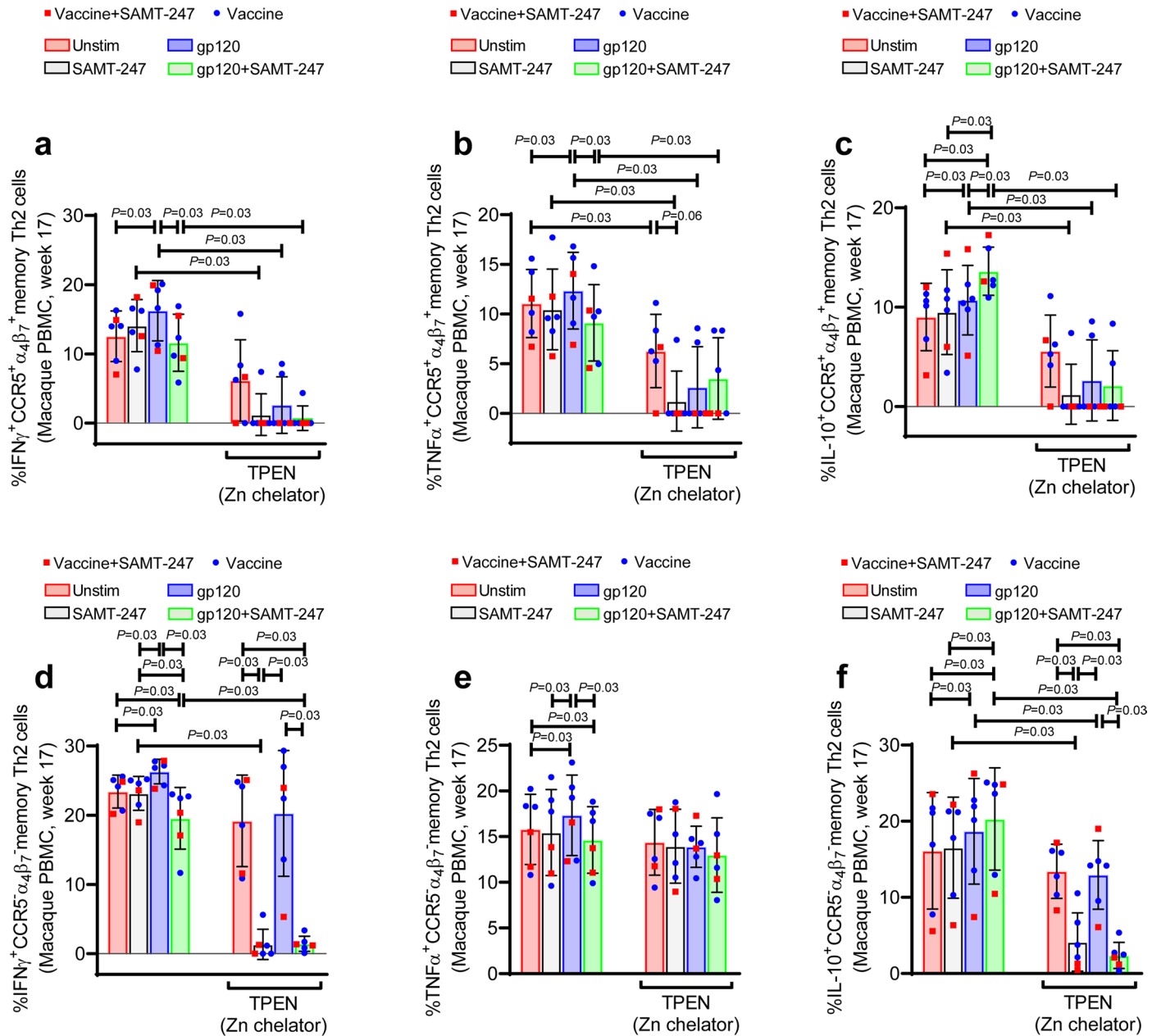
Extended Data Fig. 9 | Evaluation of cytokine responses by CCR5$^+$α$_4$β$_7^+$ and CCR5$^-$α$_4$β$_7^-$ memory Th2 cells in the presence of stimulation. a-f) Comparison of intracellular IFN-γ, TNF-α, and IL-10 cytokines by CCR5$^+$α$_4$β$_7^+$ and CCR5$^-$α$_4$β$_7^-$ Th2 memory cells in the absence or presence of zinc chelator and stimuli in the vaccine+SAMT-247 group (n = 4) and vaccine group (n = 2). Data shown in (**a-f**) were analyzed with the two-tailed Wilcoxon signed-rank test. Horizontal and vertical bars denote mean and SD.

Extended Data Table 1 | Effect of SMAT-247 and zinc chelator on different cell types in the presence or absence of different stimuli

a. Effect of SAMT-247 on NK cell and monocyte function.

Cell type	Stimulation	Cytokine		Function	
NKG2A$^+$ Blood (Vaccinated monkey)	gp120+SAMT-247	Granzyme/Perforin	↑	ADCC	↑
NKG2A$^+$ Mucosa (Age-matched monkey)	PMA+SAMT-247	Granzyme/Perforin	↑	ADCC	↑
NKG2A$^+$ Blood (Vaccinated monkey)	gp120+SAMT-247	IFN-γ *	↓	Inflammation	↓
NKG2A$^+$ Mucosa (Age-matched monkey)	PMA+SAMT-247	IFN-γ *	↓	Inflammation	↓
NKG2A$^+$ Mucosa (Age-matched monkey)	PMA+SAMT-247	TNF-α *	↓	Inflammation	↓
NKp44$^+$ Mucosa (Age-matched monkey)	PMA+SAMT-247	IL-17	↑	Epithelium homeostasis	↑
CD14$^+$ Blood (Vaccinated monkey)	gp120+SAMT-247	IL-10 *	↑	Efferocytosis	↑

* Zinc dependence

b. Effect of PMA or PMA+SAMT-247 on mucosal Th1 or Th2 cytokines.

	Unstimulated vs PMA	Unstimulated vs PMA+SAMT-247	PMA vs PMA+SAMT-247
Th1	> IFN-γ	> IFN-γ	
	>TNF-α	>TNF-α	<TNF-α
	>IL-10	>IL-10	<IL-10
Th2	>IFN-γ	> IFN-γ	
	> TNF-α	>TNF-α	<TNF-α
	>IL-10	>IL-10	

c. Effect of the zinc chelator TPEN on NK CD14$^+$ and T cell marker expression

Cytokine	Cell	Unstimulated	SAMT-247	gp120 pooled peptides	gp120 pooled peptides+SAMT-247
Granzyme B$^+$	NKG2A$^+$	-	-	-	-
Perforin$^+$	NKG2A$^+$	-	-	-	-
Survival	CD14$^+$	-	↓	↓	↓
IFN-γ$^+$	NKG2A$^+$	-	-	↓	↓
	Th1$^+$	-	↓	-	↓
	Th1$^+$CCR5$^+$α$_4$β$_7$$^+$	↓	↓	↓	↓
	Th1$^+$CCR5$^-$α$_4$β$_7$$^-$	-	↓	↓	↓
	Th2$^+$	-	↓	↓	↓
	Th2$^+$CCR5$^+$α$_4$β$_7$$^+$	-	↓	↓	↓
	Th2$^+$CCR5$^-$α$_4$β$_7$$^-$	-	↓	-	↓
TNF-α$^+$	NKG2A$^+$	-	-	↓	↓
	Th1$^+$	-	↓	↓	-
	Th1$^+$CCR5$^+$α$_4$β$_7$$^+$	-	↓	↓	-
	Th1$^+$CCR5$^-$α$_4$β$_7$$^-$	-	↓	-	↓
	Th2$^+$	-	↓	-	↓
	Th2$^+$CCR5$^+$α$_4$β$_7$$^+$	↓	↓	↓	↓
	Th2$^+$CCR5$^-$α$_4$β$_7$$^-$	-	-	-	-
IL-10$^+$	CD14$^+$	-	↓	↓	↓
	Th1$^+$	-	↓	-	↓
	Th1$^+$CCR5$^+$α$_4$β$_7$$^+$	↓	↓	↓	↓
	Th1$^+$CCR5$^-$α$_4$β$_7$$^-$	↓	↓	↓	↓
	Th2$^+$	-	↓	-	↓
	Th2$^+$CCR5$^+$α$_4$β$_7$$^+$	↓	↓	↓	↓
	Th2$^+$CCR5$^-$α$_4$β$_7$$^-$	-	↓	↓	↓

a) Effect of SAMT-247 on NK cell and monocyte function. b) Effect of PMA or PMA+SAMT-247 on mucosal Th1 or Th2 cytokines. c) Effect of the zinc chelator TPEN on NK CD14$^+$ and T cell marker expression

nature portfolio

Corresponding author(s): Genoveffa Franchini

Last updated by author(s): Feb 15, 2023

Reporting Summary

Nature Portfolio wishes to improve the reproducibility of the work that we publish. This form provides structure for consistency and transparency in reporting. For further information on Nature Portfolio policies, see our Editorial Policies and the Editorial Policy Checklist.

Statistics

For all statistical analyses, confirm that the following items are present in the figure legend, table legend, main text, or Methods section.

n/a	Confirmed	
☐	☒	The exact sample size (n) for each experimental group/condition, given as a discrete number and unit of measurement
☐	☒	A statement on whether measurements were taken from distinct samples or whether the same sample was measured repeatedly
☐	☒	The statistical test(s) used AND whether they are one- or two-sided *Only common tests should be described solely by name; describe more complex techniques in the Methods section.*
☐	☒	A description of all covariates tested
☐	☒	A description of any assumptions or corrections, such as tests of normality and adjustment for multiple comparisons
☐	☒	A full description of the statistical parameters including central tendency (e.g. means) or other basic estimates (e.g. regression coefficient) AND variation (e.g. standard deviation) or associated estimates of uncertainty (e.g. confidence intervals)
☐	☒	For null hypothesis testing, the test statistic (e.g. F, t, r) with confidence intervals, effect sizes, degrees of freedom and P value noted *Give P values as exact values whenever suitable.*
☒	☐	For Bayesian analysis, information on the choice of priors and Markov chain Monte Carlo settings
☐	☒	For hierarchical and complex designs, identification of the appropriate level for tests and full reporting of outcomes
☐	☒	Estimates of effect sizes (e.g. Cohen's d, Pearson's r), indicating how they were calculated

Our web collection on statistics for biologists contains articles on many of the points above.

Software and code

Policy information about availability of computer code

Data collection	FACSymphony A5 and examined using FACSDiva software (BD Biosciences). Confocal laser-scanning microscope (Leica SP8, Leica Microsystems, Buffalo Grove, Illinois, USA) Molecular Devices E-max plate reader (San Jose, California, USA) Droplet digital PCR
Data analysis	FlowJo software 10.6, Graph pad Prism 8.0, Imaris 9.2.1,

For manuscripts utilizing custom algorithms or software that are central to the research but not yet described in published literature, software must be made available to editors and reviewers. We strongly encourage code deposition in a community repository (e.g. GitHub). See the Nature Portfolio guidelines for submitting code & software for further information.

Data

Policy information about availability of data

All manuscripts must include a data availability statement. This statement should provide the following information, where applicable:
- Accession codes, unique identifiers, or web links for publicly available datasets
- A description of any restrictions on data availability
- For clinical datasets or third party data, please ensure that the statement adheres to our policy

All data are provided in the manuscript and supplemental material are provided in the "Source Data" file.

Human research participants

Reporting on sex and gender	Human PBMC were collected from healthy donor. The data regarding sex and gender were not shared with the authors.
Population characteristics	The authors don't have access to the data.
Recruitment	The authors were blinded regarding the recruitment of the healthy human donors. The donors were recruited by NIH blood bank.
Ethics oversight	Human PBMCs were obtained from eight healthy donors on an IRB-approved NIH protocol (99-CC-0168). Research blood donors provided written informed consent and blood samples were de-identified prior to distribution." Clinical Trials Number: NCT00001846.

Note that full information on the approval of the study protocol must also be provided in the manuscript.

Field-specific reporting

Please select the one below that is the best fit for your research. If you are not sure, read the appropriate sections before making your selection.

☒ Life sciences   ☐ Behavioural & social sciences   ☐ Ecological, evolutionary & environmental sciences

For a reference copy of the document with all sections, see nature.com/documents/nr-reporting-summary-flat.pdf

Life sciences study design

All studies must disclose on these points even when the disclosure is negative.

Sample size	Sample size was determined via consultation with our statistician. 50 macaques were divided into four groups as follows: I: 20 macaques; vaccine-microbicide group II: 18 macaques; vaccine only group III: 6 macaques; microbicide only group IV: 6 macaques control group. Group sizes were determined based on a previous vaccine study comparing 14 vaccinated macaques and 18 controls, and on a pilot experiment in which we defined a time between microbicide administration and viral challenge which would decrease the microbicide efficacy so that we could observe an additive/Synergistic effect. Historical control macaques and microbicide macaques were also used in statistical analysis as indicated. Infection rates were assumed to equal the previously observed gel only and microbicide groups, 0.333 and 0.133, respectively, and rates of 0.120 and 0.040 in the vaccine and combination groups. The last three are expected treatment efficacies of 60%, 64%, and 88%, relative to the gel only group. If the animals are given up to 14 viral challenges and the numbers of challenges to infection are compared using the Wald test of the proportional hazards model with all four groups analyzed together, then the power of the test at the two-sided 0.05 level between the vaccine group and the combination group was expected to be 79%, while the comparisons of these two groups individually vs the control group will have 82% and 99% power. The test of the microbicide group vs the combination group will have 63% power.
Data exclusions	No data were excluded.
Replication	The nature of the samples analyzed in the present studies, the limited amount of each sample collected from each animal and the cost of the non-human primate studies do not allow us to replicate the experiments. In the reported assays the replicates are represented by each animal enrolled in the study. All the data have been obtained with validated assays that have been used in previous publish work.
Randomization	50 macaques were randomized into 4 groups based on their weight, age and gender: Vaccine/microbicide group (20 macaques), Vaccine only group (n=18), microbicide only group (n=6), and control group (n=6). When samples were available we performed experiment using all the samples. For other experiments where samples were limited, samples were picked randomly from each group. For each in vitro study, samples from each animals received all the different stimulation.
Blinding	The animal handlers were blinded to the vaccine groups. Always as possible, the investigators were blinded for in vitro assays. The data analyzes were unblinded. The authors compared the immune responses between different group of animals and for that unblinded was necessary. All the in vitro study was performed blinded. During analysis of data, such as correlation and comparison of different group response, the data were unblinded.

Reporting for specific materials, systems and methods

We require information from authors about some types of materials, experimental systems and methods used in many studies. Here, indicate whether each material, system or method listed is relevant to your study. If you are not sure if a list item applies to your research, read the appropriate section before selecting a response.

Materials & experimental systems

n/a	Involved in the study
☐	☒ Antibodies
☒	☐ Eukaryotic cell lines
☒	☐ Palaeontology and archaeology
☐	☒ Animals and other organisms
☒	☐ Clinical data
☒	☐ Dual use research of concern

Methods

n/a	Involved in the study
☒	☐ ChIP-seq
☐	☒ Flow cytometry
☒	☐ MRI-based neuroimaging

Antibodies

Antibodies used

Rectal mucosal NK/ILC phenotyping and cytokine expression upon gp120 peptides/PMA stimulation in vaccinated animals.
Live/Dead Aqua Dye (cat. #L34966, 0.5 µl) from Thermo Fisher
Alexa 700 anti-CD3 (SP34-2; cat. #557917, 5µl), Alexa 700 anti-CD20 (2H7; cat. #560631, 5µl), Alexa 700 anti-CD11b (ICRF44; cat. #557918, 5µl), APC-Cy7 anti-CD16 (3G8; cat. #557758, 5µl), PE-CF594 anti-CD56 (B159; cat. #562289, 5µl) BV650 anti-NKp44 (P44-8; cat. #744302, 5µl), BV786 anti-CD45 (D058-1283; cat. #563861,5 µl) from BD Biosciences (San Jose, California, USA); and PE-Cy7 anti-NKG2A (Z199; cat. # B10246, 5µl) from Beckman Coulter (Brea, California, USA) ;FOX3-transcription buffer set (cat. #00-5523-00) from eBioscience (San Diego, California, USA); BV421 anti-IFN-γ (B27; cat. #562988, 5µl) from BD Biosciences and PE-Cy5.5 anti-IL-17 (BL168; cat. # 512314, 5µl) from BioLegend (San Diego, California, USA)

CD4+ T-cell phenotypes
LIVE/DEAD™ Fixable Blue Dead Cell Stain (cat. #L23105, Thermo Fisher); Alexa 700 anti-CD3 (SP34-2; cat. #557917, 5µl), BV785 anti-CD4 (L200; cat. #563914, 5µl), PeCy5 anti-CD95 (DX2; cat. #559773, 5µl), BV650 anti-CCR5 (3A9; cat. #564999, 5µl), BUV496 anti-CD8 (RPA-T8; cat. #564804, 5µl), BUV737 anti-CD28 (CD28.2; cat. #612815, 5µl) and FITC anti-Ki67 (B56; cat. #556026, 5µl) from BD Biosciences; APC Cy7 anti-CXCR3 (G025H7; cat. #353722, 5µl), BV605 anti-CCR6 (G034E3; cat. #353420, 5µl), BV510 anti-CD127 (A019D5; cat. #351332, 5µl), BV750 anti-PD-1 (EH12.2H7; cat. #329965, 5µl) and BV711 anti-CD25 (BC96; cat. #302636, 5µl) from BioLegend; PE-eFluor 610 anti-CXCR5 (MU5UBEE; cat. #61-9185-42, 5µl), eFluor 450 anti-FoxP3 (236A/E7; cat. #48-4777-42, 5µl) from eBioscience; and APC anti-α4β7, provided by the NIH Nonhuman Primate Reagent Resource (R24 OD010976, and NIAID contract HHSN272201300031C).

Intracellular cytokines of Human blood NK cells using SAMT-247 and PMA stimulation with or without zinc chelator.
BUV737 anti-CD3 (SP34-2; cat. #741872, 5µl), Alexa700 anti-CD20 (2H7; cat. #560631, 5µl), BV786 anti-CD45 (HI30; cat. #563716, 5µl) from BD Biosciences; APC-H7 anti-CD11b (ICRF44; cat. #47-0118-42, 5µl) from eBioscience and PE-Cy7 anti-NKG2A (Z199; cat. # B10246, 5µl) from Beckman Coulter; FOX3-transcription buffer set (cat. #00-5523-00) from eBioscience; BV750 anti-TNF-α (MAB11; cat. #566359, 5µl), BUV396 anti-IFN-γ (B27; cat. #563563, 5µl), BV510 anti-GranB (GB11; cat. #563388, 5µl) from BD Biosciences; and FITC anti-Perforin (pf-344; cat. #3465-7, 5µl) from MABTECH

AIM assay
CD40 blocking antibody (HB14, cat. # 130-094-133, 5µl) from Miltenyi; CD49a (9F10, cat. # 555501, 2µl) and CD28 (CD28.2, cat. # 567117, 2µl) from BD Bioscience; LIVE/DEAD™ Fixable Blue Dead Cell Stain (cat. #L23105, Thermo Fisher); BV786 anti-CD45 (D058-1283; cat. # 563861, 5µl), BUV737 anti-CD3 (SP34-2; cat. # 741872, 5µl), BV711 anti-CD4 (L200; cat. # 740807, 5µl), BUV496 anti-CD8 (RPA-T8; cat. # 612942, 5µl), PE-CF594 anti-PDL1 (MIH1; cat. # 563742, 5µl), BB700 anti-CTLA-4 (BNI3; cat. # 566901, 5µl), PE-Cy5 anti- OX40 (CD134) (ACT35; cat. # 551500, 5µl), BUV563 anti-CD40L (CD154) (24-31; cat. # 752854, 5µl), PE-Cy7 anti- CD69 (FN50; cat. # 557745, 5µl), PE anti- CD95 (DX2; cat. # 555674, 5µl) from BD Bioscience; FITC anti-LAG3 (3DS223H; cat. #369326, 5µl) from Thermofisher; BV750 anti-PD1 (EH12.2H7; cat. # 329966, 5µl), Alexa700 anti-CXCR3 (G025H7; cat. # 353742, 5µl), BV605 anti-CCR6 (G034E3; cat. #353420, 5µl) from Biolegend; FOX3-transcription buffer set (cat. #00-5523-00) from eBioscience (San Diego, California, USA); BV510 anti-Ki67 (B56; cat. # 563462, 5µl) from BD Biosciences

Intracellular cytokines of macaque blood NK cells and T-cells using SAMT-247 and PMA stimulation with or without zinc chelator.
Live/Dead Blue dye (cat. #L34962, 0.5µl) from Thermo Fisher; followed by surface staining with the following: PE anti-CD45 (D058-1283; cat. #552833, 5µl), BB700 anti-CD3 (RPA-T8; cat. #566452, 5µl), Alexa 700 anti-CD3 (SP34-2; cat. #557917, 5µl), BV711 anti-CD4 (L200; cat. #563913, 5µl), BV786 anti-CCR5 (3A9; cat. #565001, 5µl), BUV737 anti-CD20 (2H7; cat. #612848, 5µl), BUV496 anti-CD16 (3G8; cat. #612944, 5µl), BUV661 anti-HLA-DR (G46-6; cat. #612980, 5µl), BUV805 anti-CD14 (M5E2; cat. #565779, 5µl) from BD Biosciences; APC-H7 anti-CD11b (ICRF44; cat. #47-0118-42, 5µl), PE-Cy5 anti-CD95 (DX2; cat. #15-0959-42, 5µl) from eBioscience; PE-Cy7 anti-NKG2A (Z199; cat. # B10246, 5µl) from Beckman Coulter; APC anti-α4β7 (A4B7R1; cat. # 051514AB, 5µl) by the NIH Nonhuman Primate Reagent Resource (R24 OD010976, and NIAID contract HHSN272201300031C), and BV605 anti-CCR6 (G034E3; cat. # 353420, 5µl), BV650 anti-CXCR3 (G025H7; cat. # 353730, 5µl) from BioLegend; FOX3-transcription buffer set (cat. #00-5523-00) from eBioscience; BV750 anti-TNF-α (MAB11; cat. #566359, 5µl), BUV396 anti-IFN-γ (B27; cat. #563563, 5µl), BV510 anti-GranB (GB11; cat. #563388, 5µl), BV421 anti-IL-10 (JES3-9D7; cat. #564053, 5µl), PE-CF594 anti-Ki67 (B56; cat. #567120, 5 µl) from BD Biosciences; and FITC anti-Perforin (pf-344; cat. #3465-7, 5 µl) from MABTECH

Frequencies and cytokine levels of macaque rectal mucosal NK cells and T-cells following SAMT-247 and PMA stimulation
Live/Dead Blue dye (cat. #L34962, 0.5µl) from Thermo Fisher; followed by surface staining with the following: BUV737 anti-CD3 (SP34-2; cat. #741872, 5µl), BV711 anti-CD4 (L200; cat. #563913, 5µl), BV650 anti-NKp44 (P44-8; cat. #744302, 5µl), Alexa700 anti-CD20 (2H7; cat. #560631, 5µl), BV786 anti-CD45 (D058-1283; cat. #563861, 5µl) from BD Biosciences; APC-H7 anti-CD11b (ICRF44; cat. #47-0118-42, 5µl), PE-Cy5 anti-CD95 (ICRF44; cat. #15-0959-42, 5µl) from eBioscience; BV570 anti-CD8 (RPA-T8; cat. #301038, 5µl), BV605 anti-CCR6 (G034E3; cat. #353420, 5µl), APC anti-CXCR3 (G025H7; cat. #353708, 5µl), from BioLegend and PE-Cy7 anti-

NKG2A (Z199; cat. # B10246, 5µl) from Beckman Coulter, FOX3-transcription buffer set (cat. #00-5523-00) from eBioscience; BV750 anti-TNF-α (MAB11; cat. #566359, 5µl), BUV395 anti-IFN-γ (B27; cat. #563563, 5µl), BV510 anti-GranB (GB11; cat. #563388, 5µl), BV421 anti-IL-10 (JES3-9D7; cat. # 564053, 5µl) from BD Biosciences; PE-Cy5.5 anti-IL-17 (BL168; cat. # 512314, 5µl) from BioLegend; and FITC anti-Perforin (pf-344; cat. #3465-7, 5µl) from MABTECH

Validation

Marker Clone   Validated website
1 CD40 HB14 https://www.nhpreagents.org/ReactivityDatabase
2 CD49a 9F10 https://www.bdbiosciences.com/en-us/products/reagents/flow-cytometry-reagents/research-reagents/single-color-antibodies-ruo/pe-cy-5-mouse-anti-human-cd49d.559880
3 CD45 D058-1283 https://www.bdbiosciences.com/en-us/products/reagents/flow-cytometry-reagents/research-reagents/single-color-antibodies-ruo/pe-mouse-anti-nhp-cd45.552833
4 CD3 SP34-2 https://www.citeab.com/antibodies/2412955-557757-bd-pharmingen-apc-cy-7-mouse-anti-human-cd3?des=080d3bb9991f1653
5 CD20 2H7 https://www.bdbiosciences.com/en-us/products/reagents/flow-cytometry-reagents/research-reagents/single-color-antibodies-ruo/pe-cf594-mouse-anti-human-cd20.562295
6 CD11b ICRF44 https://www.thermofisher.com/us/en/home/life-science/cell-analysis/cell-analysis-learning-center/cell-analysis-resource-library/ebioscience-resources/human-antibody-cross-reactivity-chart.html
7 CD16 3G8 https://www.thermofisher.com/us/en/home/life-science/cell-analysis/cell-analysis-learning-center/cell-analysis-resource-library/ebioscience-resources/human-antibody-cross-reactivity-chart.html
8 CD56 B159 https://www.nhpreagents.org/ReactivityDatabase
9 NKp44 P44-8 https://www.biolegend.com/en-us/products/apc-anti-human-cd336-nkp44-antibody-3850
10 NKG2A Z199 https://www.beckman.com/reagents/coulter-flow-cytometry/antibodies-and-kits/single-color-antibodies/cd159a/a60797
11 CCR5 3A9 https://www.bdbiosciences.com/en-us/products/reagents/flow-cytometry-reagents/research-reagents/single-color-antibodies-ruo/purified-mouse-anti-human-cd195.556041
12 CD28 CD28.2 https://www.bdbiosciences.com/en-us/products/reagents/functional-cell-based-reagents/purified-na-le-mouse-anti-human-cd28.567117
13 CD4 L200 https://www.bdbiosciences.com/en-us/products/reagents/flow-cytometry-reagents/research-reagents/single-color-antibodies-ruo/fitc-mouse-anti-human-cd4.550628
14 CD8 RPA-T8 https://www.thermofisher.com/us/en/home/life-science/cell-analysis/cell-analysis-learning-center/cell-analysis-resource-library/ebioscience-resources/human-antibody-cross-reactivity-chart.html
15 CD127 A019D5 https://www.citeab.com/antibodies/524313-351304-pe-anti-human-cd127-il-7r-antibody
16 PD1 EH12.1 https://www.nature.com/articles/s41586-020-03041-6
17 HLA-DR G46-6 https://www.fishersci.com/shop/products/hla-dr-mouse-anti-human-rhesus-cynomolgus-baboon-r718-clone-g46-6-also-known-as-l243-bd-horizon/p-7227060
18 CTLA-4 BNI3 https://www.citeab.com/antibodies/2408361-555851-bd-pharmingen-purified-mouse-anti-human-cd15?des=e3d22b3bfa1d8952
19 PDL1 EH12.2H7 https://www.citeab.com/antibodies/523807-329902-purified-anti-human-cd279-pd-1-antibody?des=7156e11a58406a10
20 OX40 (CD134) ACT35 https://www.abcam.com/recombinant-rhesus-monkey-cd134--ox40l-receptor-protein-active-ab221322.html?productWallTab=ShowAll
21 CD25 BC96 https://www.thermofisher.com/us/en/home/life-science/cell-analysis/cell-analysis-learning-center/cell-analysis-resource-library/ebioscience-resources/human-antibody-cross-reactivity-chart.html
22 CXCR5 MU5UBEE https://www.thermofisher.com/us/en/home/life-science/cell-analysis/cell-analysis-learning-center/cell-analysis-resource-library/ebioscience-resources/human-antibody-cross-reactivity-chart.html
23 α4β7 A4B7R1 https://www.nhpreagents.org/Store/CategoryID/1/ProductID/37
24 Ki67 B56 https://www.nhpreagents.org/ReactivityDatabase
25 IL-17 BL168 https://www.nature.com/articles/s41564-020-00841-4
26 FoxP3 236A/E7 https://www.thermofisher.com/us/en/home/life-science/cell-analysis/cell-analysis-learning-center/cell-analysis-resource-library/ebioscience-resources/human-antibody-cross-reactivity-chart.html
27 Perforin pf-344 https://www.mabtech.com/products/anti-human-perforin-antibody-pf-344-fitc-3465-7-0
28 GranB GB11 https://www.nhpreagents.org/ReactivityDatabase
29 IL-10 JES3-9D7 https://www.nhpreagents.org/ReactivityDatabase
30 CD69 FN50 https://www.thermofisher.com/us/en/home/life-science/cell-analysis/cell-analysis-learning-center/cell-analysis-resource-library/ebioscience-resources/human-antibody-cross-reactivity-chart.html
31 CD95 DX2 https://www.thermofisher.com/us/en/home/life-science/cell-analysis/cell-analysis-learning-center/cell-analysis-resource-library/ebioscience-resources/human-antibody-cross-reactivity-chart.html
32 CD40L (CD154) 24-31 https://www.nhpreagents.org/ReactivityDatabase
33 CXCR3 G025H7 https://www.biolegend.com/en-us/products/biotin-anti-human-cd183-cxcr3-antibody-13320
34 CCR6 G034E3 https://www.biolegend.com/en-us/products/purified-anti-human-cd196-ccr6-antibody-7512
35 LAG3 3DS223H https://www.citeab.com/antibodies/3246730-17-2239-42-cd223-lag-3-monoclonal-antibody-3ds223
36 IFN-γ B27 https://www.bdbiosciences.com/en-us/products/reagents/immunoassay-reagents/purified-mouse-anti-human-ifn.554699
37 CD14 M5E2 https://www.bdbiosciences.com/en-us/products/reagents/flow-cytometry-reagents/research-reagents/single-color-antibodies-ruo/apc-mouse-anti-human-cd14.561383
38 TNF-α MAB11 https://www.bdbiosciences.com/en-us/products/reagents/immunoassay-reagents/elisa/biotin-mouse-anti-human-tnf.554511

Animals and other research organisms

Laboratory animals	Fifty female Indian rhesus macaques obtained from the free-range breeding colony on Morgan Island, South Carolina, were used in this study. The macaques, aged 2 to 3 years at study initiation. One time rectal tissue samples from 9 female random rhesus macaque were collected for this project to do some in vitro study.
Wild animals	No wild animals were used in this study.
Reporting on sex	Fifty female Indian rhesus macaques were used in the study. It was necessary to use female macaques since the study tested a candidate vaccine in combination with vaginal gel containing SAMt-247 microbicide to understand the protective efficacy of the combination. the consideration of sex in this study design an interpretation of results are described throughout the text and in the on line method section. One time rectal tissue samples from 9 female random rhesus macaque were collected for this project to do some in vitro study.
Field-collected samples	No field samples were collected in this study.
Ethics oversight	The NCI (National Cancer Institute) ACUC (Animal Care and Use Committee) approved and provided guidance for the animal protocol. The 9 rectal tissue collection was approved by the Tulane Animal Care and Use Committee (ACUC).

Note that full information on the approval of the study protocol must also be provided in the manuscript.

Flow Cytometry

Plots

Confirm that:

☒ The axis labels state the marker and fluorochrome used (e.g. CD4-FITC).

☒ The axis scales are clearly visible. Include numbers along axes only for bottom left plot of group (a 'group' is an analysis of identical markers).

☒ All plots are contour plots with outliers or pseudocolor plots.

☒ A numerical value for number of cells or percentage (with statistics) is provided.

Methodology

Sample preparation	Sample preparation is described in "online methods" section. Freshly collected rectal biopsies were digested with collagenase (2 mg/ml; Sigma-Aldrich) in the absence of FBS in 370 C for 1 hour, then it was mechanically separated by using a 10ml syringe with a blunt head cannula. It was washed with R10 and pass through 70um cell strainer. Single cells were counted and used for the experiment. EDTA whole blood was layered on the top of Ficoll Plaque (GE Healthcare, Chicago, Illinois, USA), and centrifuged at 2800rmp, 30 minutes, accelerator 4 and decelerator 4. The white PBMC band was collected, washed with PBS and used for experiments. Neutrophils were isolated following isolation of PBMCs by Ficoll Plaque (GE Healthcare, Chicago, Illinois, USA), the cellular pellet was added to an equal volume of 20% dextran in water, gently mixed, and incubated for 1 min. Approximately three volumes of PBS were added, mixed again, and incubated in the dark for 50-60 minutes. At the end of incubation, the clear layer at the top of the tube containing neutrophils was collected. Cells were pelleted and treated with ACK lysing buffer (Quality Biological, Gaithersburg, MD, USA) for 5 min at 37ºC, washed with R10 and counted.
Instrument	Cytometry acquisition was done using the FACS Symphony A5 or FACS LSRII.
Software	Acquisition was done using FACSDiva software (BD Biosciences, San Jose, California, USA). Cytometry data were analysed using Flow Jo LLC, V10.6
Cell population abundance	Human NKG2A+ cells were sort with 99% purity. A starting 20-30 million cryo preserved PBMC was used for the sorting and 2-3 million NKG2A+ cells were obtained.
Gating strategy	NK/ILC gating Singlets, Live cells, CD45+, CD3-CD20-CD11b-, NKp44+/NKG2A+/NKp44-NKG2A- Th1 and Th2 Gating was done on live CD3+CD4+ cells and on vaccine induced Ki67+ cells. CXCR3 and CCR6 expression were used to identify Th1 or Th2 populations. CXCR3-CCR6- is Th2 and CXCR3+CCR6- is Th1 cells

☒ Tick this box to confirm that a figure exemplifying the gating strategy is provided in the Supplementary Information.